

Marchenko redatuming, imaging and multiple elimination, and their mutual relations

Kees Wapenaar¹, Joeri Brackenhoff^{1,2}, Marcin Dukalski³, Giovanni Meles^{1,4}, Christian Reinicke^{1,3}, Evert Slob¹, Myrna Staring^{1,5}, Jan Thorbecke¹, Joost van der Neut¹ and Lele Zhang¹

¹*Delft University of Technology, Department of Geoscience and Engineering, Stevinweg 1, 2628 CN Delft, The Netherlands*

²*ETH Zürich, Department of Earth Sciences, Sonneggstrasse 5, 8092 Zürich, Switzerland*

³*Aramco Overseas Company B.V., Informaticalaan 6-12, 2628 ZD Delft, The Netherlands*

⁴*Institute of Earth Sciences, University of Lausanne, Lausanne, 1015, Switzerland*

⁵*Fugro Innovation & Technology, Prismastraat 4, Nootdorp, The Netherlands*

Right-running head: Marchenko methods and mutual relations

(Dated: April 28, 2021)

With the Marchenko method it is possible to retrieve Green's functions between virtual sources in the subsurface and receivers at the surface from reflection data at the surface and focusing functions. A macro model of the subsurface is needed to estimate the first arrival; the internal multiples are retrieved entirely from the reflection data. The retrieved Green's functions form the input for redatuming by multidimensional deconvolution (MDD). The redatumed reflection response is free of internal multiples related to the overburden. Alternatively, the redatumed response can be obtained by applying a second focusing function to the retrieved Green's functions. This process is called Marchenko redatuming by double focusing. It is more stable and better suited for an adaptive implementation than Marchenko redatuming by MDD, but it does not eliminate the multiples between the target and the overburden. An attractive efficient alternative is plane-wave Marchenko redatuming, which retrieves the responses to a limited number of plane-wave sources at the redatuming level. In all cases, an image of the subsurface can be obtained from the redatumed data, free of artefacts caused by internal multiples. Another class of Marchenko methods aims at eliminating the internal multiples from the reflection data, while keeping the sources and receivers at the surface. A specific characteristic of this form of multiple elimination is that it predicts and subtracts all orders of internal multiples with the correct amplitude, without needing a macro subsurface model. Like Marchenko redatuming, Marchenko multiple elimination can be implemented as an MDD process, a double dereverberation process, or an efficient plane-wave oriented process. In this paper we systematically discuss the different approaches to Marchenko redatuming, imaging and multiple elimination, using a common mathematical framework.

INTRODUCTION

Building on the autofocusing method of Rose (2001, 2002), Brogгинi and Snieder (2012) showed how the Marchenko method can be used to retrieve the 1D Green's function between a virtual source in the subsurface and a receiver at the surface from the reflection response at the surface. Unlike in seismic interferometry (Campillo and Paul, 2003; Wapenaar, 2003; Schuster et al., 2004; Bakulin and Calvert, 2006; Gouédard et al., 2008), no physical receiver is needed at the position of the virtual source. The generalization of this Green's function retrieval method to 3D situations (Wapenaar et al., 2014) formed the basis for the development of Marchenko redatuming and imaging methods (Behura et al., 2014; Brogгинi et al., 2014). The main characteristic of these methods is that internal multiples are dealt with in a data-driven way. A subsurface image obtained with the Marchenko method is free of artefacts related to internal multiples. The required input consists of the reflection response at the surface (deconvolved for the seismic wavelet and free of surface-related multiples) and an estimate of the direct arrivals of the Green's functions. The lat-

ter can be obtained from a macro model of the subsurface. Hence, the required input is the same as that for standard redatuming and imaging of primary reflections; the information needed to deal with the internal multiples comes entirely from the reflection response at the surface.

Since the introduction of the Marchenko method in geophysics, many variants have been introduced. In the initial approach, redatuming was achieved by applying multidimensional deconvolution (MDD) to the downgoing and upgoing Green's functions retrieved with the Marchenko method (Broggini et al., 2014; Ravasi et al., 2016). To obtain a more stable method, suited for adaptive implementation, redatuming by double focusing was developed (van der Neut et al., 2015c; Staring et al., 2018). An important efficiency gain was achieved with the plane-wave Marchenko redatuming approach (Meles et al., 2018). In all these approaches, sources and receivers are redatumed from the surface to virtual sources and receivers at one or more depth levels in the subsurface. This requires a macro model of the overburden. To make the Marchenko method less sensitive to the macro model, it was proposed to extrapolate the virtual sources and

receivers upward to the acquisition surface (Meles et al., 2016; van der Neut and Wapenaar, 2016). This led to a class of Marchenko multiple elimination methods, i.e., methods in which the sources and receivers stay at the surface while the internal multiples are eliminated from the data (Zhang et al., 2019a,b; Pereira et al., 2019; Elison et al., 2020; Dukalski and de Vos, 2020; Meles et al., 2020; Staring et al., 2021).

In this paper we discuss the different Marchenko methods in a systematic way, show their mutual relations and discuss the specific properties of each method. By using a consistent way of presenting these methods, using a unified notation, we hope to convey the systematics of the many Marchenko methods that are currently around. The emphasis will be on explanations with cartoon-like figures. Numerical examples and field data applications can be found in the referenced literature.

It is impossible to discuss all existing Marchenko methods in a single paper. At various places we include references for variants that are not discussed here. In particular, the discussion in this paper is restricted to acoustic methods for lossless media. For a discussion of the Marchenko method in dissipative media we refer to Slob (2016) and for elastodynamic Marchenko methods to Wapenaar and Slob (2014), da Costa Filho et al. (2014) and Reinicke et al. (2020). Throughout the paper we assume that the input data are properly sampled. For Marchenko methods that compensate for the effects of irregular sampling, see Haindl et al. (2018), Peng et al. (2019) and van IJsseldijk and Wapenaar (2021). Recent developments on the integration of the Marchenko method with full waveform inversion (Cui et al., 2020; Shoja et al., 2020) and Marchenko methods without up/down decomposition (Diekman and Vasconcelos, 2021; Kiraz et al., 2021; Wapenaar et al., 2021) are also beyond the scope of this paper.

MARCHENKO REDATUMING AND IMAGING

Seismic redatuming is the process of virtually moving sources and/or receivers from the acquisition surface to a new depth level (or ‘datum plane’) in the subsurface. Traditionally this is done with one-way wave field extrapolation operators (or ‘focusing operators’) which account for primaries only (Berkhout, 1982; Berryhill, 1984). Classical wave field extrapolation and redatuming methods that account for internal multiples exist (Wapenaar et al., 1987; Mulder, 2005), but they require a very detailed subsurface model. Redatuming methods that are based on seismic interferometry (Schuster et al., 2004; Bakulin and Calvert, 2006; van der Neut et al., 2011) do not need a subsurface model, but they require the presence of actual receivers at the depth level to which one wants to redatum the sources.

Broggini and Snieder (2012) showed that with the Marchenko method the same can be achieved as with seismic interferometry, at least in 1D, without requiring actual receivers in the subsurface. This was the inspiration for the research into 3D Marchenko redatuming and imaging, which is extensively discussed in this section. Marchenko redatuming is a data-driven method to create virtual sources and receivers in the subsurface. It accounts for internal multiples in the overburden, it only needs a macro model of the overburden and it does not require the presence of actual receivers in the subsurface.

Focusing functions

The focusing function plays an essential role in the Marchenko method. It is a 3D generalization of the ‘fundamental solution’ in 1D scattering problems (Lamb, 1980). On the other hand, from the seismic perspective it can be seen as a generalization of the 3D focusing operator used in traditional redatuming, accounting for internal multiples. Here we discuss its basic properties. In the section “Retrieval of focusing functions” we show how it can be retrieved from the reflection response at the surface.

Consider a 3D inhomogeneous lossless acoustic medium, with propagation velocity $c(\mathbf{x})$ and mass density $\rho(\mathbf{x})$, where $\mathbf{x} = (x_1, x_2, x_3)$ is the Cartesian coordinate vector. Here x_1 and x_2 are the horizontal coordinates, in the following denoted by vector $\mathbf{x}_H = (x_1, x_2)$; x_3 is the depth coordinate. For 2D situations, the coordinate vectors reduce to $\mathbf{x} = (x_1, x_3)$ and $\mathbf{x}_H = x_1$, respectively. The acquisition boundary at $x_3 = x_{3,0}$ is denoted as \mathbb{S}_0 . Throughout this paper we assume that \mathbb{S}_0 is a transparent boundary and that the upper half-space is homogeneous. We choose a focal point $\mathbf{x}_A = (\mathbf{x}_{H,A}, x_{3,A})$ in the subsurface, with $\mathbf{x}_{H,A} = (x_{1,A}, x_{2,A})$ (or $\mathbf{x}_{H,A} = x_{1,A}$ in the 2D situation) and $x_{3,A} > x_{3,0}$, and define a boundary \mathbb{S}_A at the focal depth $x_{3,A}$. We define a truncated version of the medium, which is identical to the actual medium above \mathbb{S}_A and reflection free below \mathbb{S}_A . We introduce the focusing function $f_1(\mathbf{x}, \mathbf{x}_A, t)$ (with t denoting time) in this truncated medium. It consists of a downgoing part $f_1^+(\mathbf{x}, \mathbf{x}_A, t)$ and an upgoing part $f_1^-(\mathbf{x}, \mathbf{x}_A, t)$ (the superscripts + and – refer to the propagation direction at the first coordinate vector, here \mathbf{x}). The downgoing focusing function $f_1^+(\mathbf{x}_S, \mathbf{x}_A, t)$, with \mathbf{x}_S at \mathbb{S}_0 , is defined such that $f_1^+(\mathbf{x}, \mathbf{x}_A, t)$ focuses at $\mathbf{x} = \mathbf{x}_A$ and $t = 0$ and continues as a diverging downgoing field into the reflection-free half-space below \mathbb{S}_A . The upgoing focusing function $f_1^-(\mathbf{x}_R, \mathbf{x}_A, t)$ is the response of the truncated medium to $f_1^+(\mathbf{x}_S, \mathbf{x}_A, t)$, observed at \mathbf{x}_R at \mathbb{S}_0 . Both the downgoing and upgoing functions are visualized in Figure 1a. Note that downgoing and upgoing waves meet each other at interfaces in such a way that only

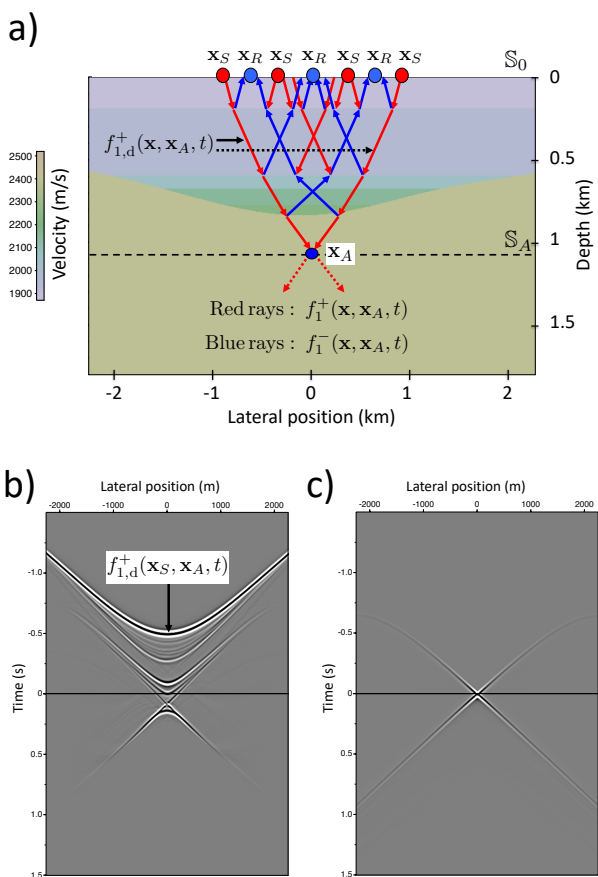


FIG. 1 (a) Focusing functions f_1^+ and f_1^- in the truncated medium. (b) The focusing function $f_1^+(\mathbf{x}_S, \mathbf{x}_A, t)$ (fixed \mathbf{x}_A , variable \mathbf{x}_S) with \mathbf{x}_S at \mathbb{S}_0 and \mathbf{x}_A at \mathbb{S}_A . (c) The focused field $f_1^+(\mathbf{x}'_A, \mathbf{x}_A, t)$ (fixed \mathbf{x}_A , variable \mathbf{x}'_A) with \mathbf{x}'_A and \mathbf{x}_A at \mathbb{S}_A .

the direct arrival of the focusing function, denoted by $f_{1,d}^+(\mathbf{x}, \mathbf{x}_A, t)$, reaches the focal point.

The propagation of the focusing function through the truncated medium, from \mathbb{S}_0 to \mathbb{S}_A , is formally described by

$$f_1^+(\mathbf{x}'_A, \mathbf{x}_A, t) = \int_{\mathbb{S}_0} d\mathbf{x}_S \int_0^\infty T(\mathbf{x}'_A, \mathbf{x}_S, t') f_1^+(\mathbf{x}_S, \mathbf{x}_A, t - t') dt', \quad (1)$$

for \mathbf{x}'_A at \mathbb{S}_A , where $T(\mathbf{x}'_A, \mathbf{x}_S, t)$ is the transmission response of the truncated medium. Throughout the paper we assume that downgoing and upgoing fields are power-flux normalized (Frasier, 1970; Kennett et al., 1978; Ursin, 1983; Chapman, 1994), which explains why expressions like equation 1 do not contain the vertical spatial derivative of one of the functions under the integral. The formal focusing conditions are

$$f_1^+(\mathbf{x}'_A, \mathbf{x}_A, t) = \delta(\mathbf{x}'_{H,A} - \mathbf{x}_{H,A}) \delta(t), \quad (2)$$

$$f_1^-(\mathbf{x}'_A, \mathbf{x}_A, t) = 0, \quad (3)$$

for \mathbf{x}'_A at \mathbb{S}_A . From equations 1 and 2 it follows that $f_1^+(\mathbf{x}_S, \mathbf{x}_A, t)$ is by definition the inverse of $T(\mathbf{x}_A, \mathbf{x}_S, t)$. For the truncated medium of Figure 1a, the downgoing function $f_1^+(\mathbf{x}_S, \mathbf{x}_A, t)$, convolved with a wavelet, is shown in grey-level display in Figure 1b. Its direct contribution $f_{1,d}^+(\mathbf{x}_S, \mathbf{x}_A, t)$ is a hyperbolic-like event at negative time (actually this is the traditional one-way focusing operator (Berkhout and Wapenaar, 1993)). If no scattering occurred between \mathbb{S}_0 and \mathbb{S}_A , this would be the complete focusing function. However, in a scattering medium, additional events are present in $f_1^+(\mathbf{x}_S, \mathbf{x}_A, t)$ (as visualized in Figures 1a and 1b), which avoid that multiply scattered waves reach \mathbb{S}_A . Figure 1c shows the focused field $f_1^+(\mathbf{x}'_A, \mathbf{x}_A, t)$, with \mathbf{x}'_A at \mathbb{S}_A , obtained by emitting $f_1^+(\mathbf{x}_S, \mathbf{x}_A, t)$ (convolved with a wavelet) into the truncated medium, according to equation 1. The amplitudes are clipped to emphasize the details. Note that there are no artefacts related to multiple scattering. Nevertheless, the focused field deviates from the desired result, expressed by equation 2. The explanation is that, in practical situations, the aperture is finite and focusing functions do not compensate for evanescent waves, which implies a spatial band-limitation (Berkhout and van Wulfften Palthe, 1979, App. C). Moreover, in practice the seismic wavelet implies a temporal band-limitation. Hence, the delta functions in equation 2 (and in the remainder of the paper) should be interpreted as band-limited delta functions. Consequently, in practice the downgoing focusing function $f_1^+(\mathbf{x}_S, \mathbf{x}_A, t)$ is actually a band-limited inverse of the transmission response $T(\mathbf{x}_A, \mathbf{x}_S, t)$.

Representations

We discuss two representations, which formulate mutual relations between Green's functions and the focusing functions introduced in the previous section. First we introduce the decomposed Green's functions $G^{-,+}(\mathbf{x}_R, \mathbf{x}_A, t)$ and $G^{-,-}(\mathbf{x}_R, \mathbf{x}_A, t)$, with \mathbf{x}_A at \mathbb{S}_A inside the medium and \mathbf{x}_R at the acquisition boundary \mathbb{S}_0 , see Figure 2a. Unlike the focusing functions, the Green's functions are defined in the actual medium, which in general is inhomogeneous also below \mathbb{S}_A . Following common conventions, the second coordinate vector (here \mathbf{x}_A) denotes the position of the impulsive source and the first coordinate vector (here \mathbf{x}_R) that of the receiver. In the same order, the superscripts denote the propagation directions at the source and receiver. Since the half-space above \mathbb{S}_0 is homogeneous, only upgoing waves arrive at the receiver.

For a source at \mathbf{x}_S at the acquisition boundary \mathbb{S}_0 , the Green's function $G^{-,+}(\mathbf{x}_R, \mathbf{x}_S, t)$ is by definition the reflection response of the medium. We denote this by $R(\mathbf{x}_R, \mathbf{x}_S, t)$. The following relations hold between

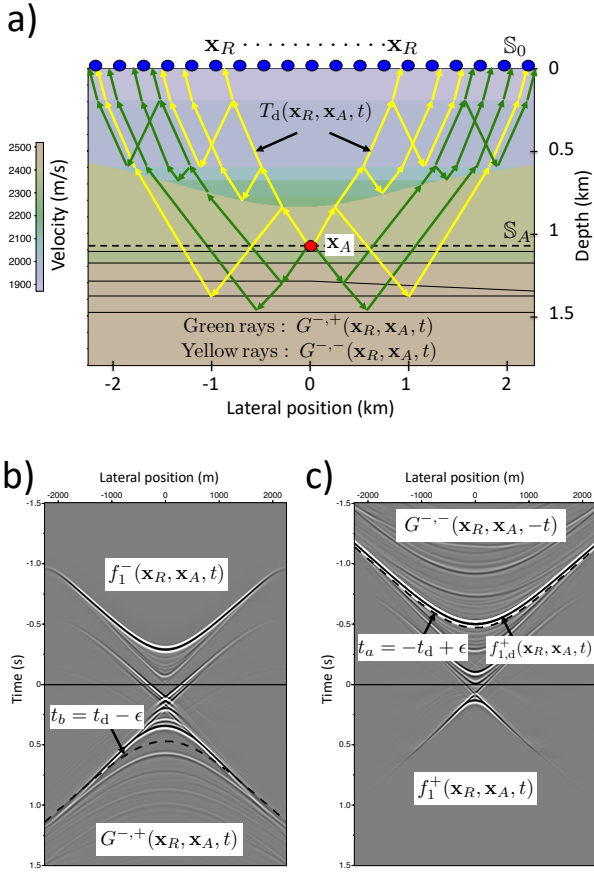


FIG. 2 (a) Green's functions in the actual medium. (b) The left-hand side of equation 4 (fixed \mathbf{x}_A , variable \mathbf{x}_R). (c) The left-hand side of equation 5.

the power-flux normalized Green's functions and focusing functions (Slob et al., 2014; Wapenaar et al., 2014)

$$G^{-,+}(\mathbf{x}_R, \mathbf{x}_A, t) + f_1^-(\mathbf{x}_R, \mathbf{x}_A, t) = \int_{\mathbb{S}_0} d\mathbf{x}_S \int_0^\infty R(\mathbf{x}_R, \mathbf{x}_S, t') f_1^+(\mathbf{x}_S, \mathbf{x}_A, t - t') dt' \quad (4)$$

and

$$G^{-,-}(\mathbf{x}_R, \mathbf{x}_A, -t) + f_1^+(\mathbf{x}_R, \mathbf{x}_A, t) = \int_{\mathbb{S}_0} d\mathbf{x}_S \int_{-\infty}^0 R(\mathbf{x}_R, \mathbf{x}_S, -t') f_1^-(\mathbf{x}_S, \mathbf{x}_A, t - t') dt', \quad (5)$$

see also the Appendix. The time integration boundaries acknowledge the fact that the reflection response $R(\mathbf{x}_R, \mathbf{x}_S, t)$ is a causal function of time, i.e., $R(\mathbf{x}_R, \mathbf{x}_S, t < 0) = 0$. Both equations account for internal multiple scattering. Equation 4 is exact, whereas in equation 5 evanescent waves are neglected. The interpretation of equation 4 is as follows. The right-hand side quantifies the reflection response of the actual medium to the downgoing focusing function $f_1^+(\mathbf{x}_S, \mathbf{x}_A, t)$. The left-hand side shows that this

reflection response consists of the upgoing focusing function $f_1^-(\mathbf{x}_R, \mathbf{x}_A, t)$ (the blue rays arriving at \mathbb{S}_0 in Figure 1a) and the Green's function $G^{-,+}(\mathbf{x}_R, \mathbf{x}_A, t)$. The latter can be understood as follows. In Figure 1a it can be seen that the focal point \mathbf{x}_A acts as a virtual source at $t = 0$ for downgoing waves. Figure 2a shows that the response to this virtual source is the Green's function $G^{-,+}(\mathbf{x}_R, \mathbf{x}_A, t)$ (the green rays in this figure). Equation 5 is interpreted in a similar way. The right-hand side quantifies the reflection response of the time-reversed actual medium to the upgoing focusing function $f_1^-(\mathbf{x}_S, \mathbf{x}_A, t)$. The left-hand side shows that this reflection response consists of the downgoing focusing function $f_1^+(\mathbf{x}_R, \mathbf{x}_A, t)$ and the time-reversed Green's function $G^{-,-}(\mathbf{x}_R, \mathbf{x}_A, -t)$. The functions on the left-hand sides of equations 4 and 5, convolved with a wavelet, are shown in grey-level display in Figures 2b and 2c, respectively.

Recall that we assume that \mathbb{S}_0 is a transparent boundary and that the half-space above \mathbb{S}_0 is homogeneous. Hence, the reflection response R in equations 4 and 5 contains no surface-related multiples, which complies with the situation after surface-related multiple elimination (Verschuur et al., 1992; van Groenestijn and Verschuur, 2010). Alternatively, equations 4 and 5 can be modified to account for surface-related multiples in R (see Ware and Aki (1969) for the 1D situation and Singh et al. (2017) and Dukalski and de Vos (2018) for 2D and 3D situations). A further discussion on the inclusion of surface-related multiples in the representations is beyond the scope of this paper.

Retrieval of focusing functions

Assuming R is known, equations 4 and 5 form a system of two equations for four unknowns (f_1^+ , f_1^- , $G^{-,+}$ and $G^{-,-}$). An inspection of Figures 2b and 2c reveals that the Green's functions reside in other time intervals than the focusing functions. We discuss window functions to suppress the Green's functions from equations 4 and 5, so that we are left with a system of two equations for two unknowns. To define a time window for equation 4, we need to know the first possible arrival of $G^{-,+}(\mathbf{x}_R, \mathbf{x}_A, t)$. This would occur when there would be a reflector just below \mathbb{S}_A . For the first possible arrival of this Green's function we write

$$\{G^{-,+}(\mathbf{x}_R, \mathbf{x}_A, t)\}_{\text{first}} \propto T_d(\mathbf{x}_R, \mathbf{x}_A, t), \quad (6)$$

where 'first' stands for 'first possible', T_d is the direct arrival of the transmission response of the medium between \mathbb{S}_A and \mathbb{S}_0 (which is also the direct arrival of $G^{-,-}$, see Figure 2a), and \propto stands for 'proportional to'. Note that we ignored the reflection coefficient of the hypothetical reflector (this is justified since we only use equation 6 to derive the time window). We denote the arrival time of the direct transmission

response as $t_d(\mathbf{x}_R, \mathbf{x}_A)$. Hence, $G^{-,+}(\mathbf{x}_R, \mathbf{x}_A, t)$ can be suppressed from equation 4 by applying a time window that removes everything beyond $t = t_b = t_d(\mathbf{x}_R, \mathbf{x}_A) - \epsilon$ (the dashed line in Figure 2b). Here ϵ is a small positive time constant (typically half the duration of a wavelet), to account for the fact that in practice all terms in equations 4 and 5 are band-limited. To define a time window for equation 5, we need to know the last arrival of the time-reversed Green's function $G^{-,-}(\mathbf{x}_R, \mathbf{x}_A, -t)$. This is given by the time-reversed direct arrival, hence

$$\{G^{-,-}(\mathbf{x}_R, \mathbf{x}_A, -t)\}_{\text{last}} = -T_d(\mathbf{x}_R, \mathbf{x}_A, -t) \quad (7)$$

(the factor -1 follows from the sign-convention for the source for upgoing waves in $G^{-,-}$ (Wapenaar, 1996), but this sign is irrelevant for the derivation of the time window). Hence, $G^{-,-}(\mathbf{x}_R, \mathbf{x}_A, -t)$ can be suppressed from equation 5 by applying a time window that removes everything before $t = t_a = -t_d(\mathbf{x}_R, \mathbf{x}_A) + \epsilon$ (the dashed line in Figure 2c). Note that $t_a = -t_b$. Based on this analysis, we define two time windows as

$$\Theta_a(\mathbf{x}_R, \mathbf{x}_A, t) = \theta(t - t_a) = \theta(t + t_d - \epsilon), \quad (8)$$

$$\Theta_b(\mathbf{x}_R, \mathbf{x}_A, t) = \theta(t_b - t) = \theta(t_d - \epsilon - t), \quad (9)$$

where $\theta(t)$ is the Heaviside step function (or, in practice, a tapered version of the Heaviside step function). These windows suppress the Green's functions and pass the focusing functions f_1^+ and f_1^- , except the direct arrival $f_{1,d}^+(\mathbf{x}_R, \mathbf{x}_A, t)$, which coincides with the last arrival of $G^{-,-}(\mathbf{x}_R, \mathbf{x}_A, -t)$, see Figure 2c.

A few words of caution are needed here. First, equation 6 is only correct for limited offsets: at large offsets, refracted waves in $G^{-,+}$ may arrive earlier than T_d . Second, in a laterally varying strongly scattering medium, diffraction events in the focusing functions may be unintentionally suppressed by the time windows. Third, in practice the inherent band-limitation may cause partial interference of focusing functions and Green's functions, particularly in the case of thin layers (i.e., thin compared to the wavelength). In this paper we assume that offsets are limited, lateral variations are mild, and layers are not thin. Dukalski et al. (2019) discuss how to account for thin layering, assuming the medium is horizontally layered.

Application of the window $\Theta_b(\mathbf{x}_R, \mathbf{x}_A, t)$ to both sides of equation 4 gives

$$f_1^-(\mathbf{x}_R, \mathbf{x}_A, t) = \Theta_b \int_{\mathbb{S}_0} d\mathbf{x}_S \int_0^\infty R(\mathbf{x}_R, \mathbf{x}_S, t') f_1^+(\mathbf{x}_S, \mathbf{x}_A, t - t') dt'. \quad (10)$$

Similarly, applying $\Theta_a(\mathbf{x}_R, \mathbf{x}_A, t)$ to both sides of

equation 5 we obtain

$$f_1^+(\mathbf{x}_R, \mathbf{x}_A, t) - f_{1,d}^+(\mathbf{x}_R, \mathbf{x}_A, t) = \Theta_a \int_{\mathbb{S}_0} d\mathbf{x}_S \int_{-\infty}^0 R(\mathbf{x}_R, \mathbf{x}_S, -t') f_1^-(\mathbf{x}_S, \mathbf{x}_A, t - t') dt'. \quad (11)$$

The term $-f_{1,d}^+$ on the left-hand side of equation 11 accounts for the fact that $f_{1,d}^+$ is not passed by the window, see Figure 2c. Equations 10 and 11 form a coupled system of Marchenko equations. We show how f_1^+ and f_1^- can be retrieved, assuming R and $f_{1,d}^+$ are known. We adopt the compact operator notation introduced by van der Neut et al. (2015b). In this notation, equations 10 and 11 read

$$f_1^- = \Theta_b R f_1^+, \quad (12)$$

$$f_1^+ = \Theta_a R^* f_1^- + f_{1,d}^+, \quad (13)$$

with superscript \star denoting time-reversal. For simplicity we use the same fonts for operators as for wave fields. Operations like $R f_1^+$ stand for a (multidimensional) convolution process (see right-hand side of equation 10), whereas operations containing a time-reversal, like $R^* f_1^-$, stand for a correlation process (see right-hand side of equation 11). Window functions are always applied in a multiplicative sense. Substitution of equation 12 into equation 13 gives

$$f_1^+ = \Theta_a R^* \Theta_b R f_1^+ + f_{1,d}^+. \quad (14)$$

The product notation $\Theta_a R^* \Theta_b R f_1^+$ should be understood in the sense that operators and window functions act on all terms to the right of it, hence it stands for $\Theta_a(R^*(\Theta_b(R f_1^+)))$. For notational convenience we will not use the brackets. We rewrite equation 14 as

$$\{\delta - \Theta_a R^* \Theta_b R\} f_1^+ = f_{1,d}^+, \quad (15)$$

where δ is the identity operator. This equation can be solved by

$$f_1^+ = \sum_{k=0}^K \{\Theta_a R^* \Theta_b R\}^k f_{1,d}^+, \quad (16)$$

where K is the number of iterations needed for the scheme to converge with acceptable accuracy (convergence is guaranteed for $K \rightarrow \infty$ (Dukalski and de Vos, 2018)). Other approaches to solve equation 15 are proposed by van der Neut et al. (2015a), Dukalski and de Vos (2018) and Becker et al. (2018). Once f_1^+ is found, f_1^- follows from equation 12. We call equation 16 the Marchenko scheme. As input it requires the reflection response $R(\mathbf{x}_R, \mathbf{x}_S, t)$ at the acquisition boundary (i.e., the reflection measurements after surface-related multiple elimination and deconvolution for the wavelet) and the direct arrival $f_{1,d}^+(\mathbf{x}_R, \mathbf{x}_A, t)$ of the focusing function. Analogous to equations 1 and 2, the latter is related to the direct arrival of the transmis-

sion response via

$$\delta(\mathbf{x}'_{H,A} - \mathbf{x}_{H,A})\delta(t) = \int_{\mathbb{S}_0} d\mathbf{x}_R \int_0^\infty T_d(\mathbf{x}'_A, \mathbf{x}_R, t') f_{1,d}^+(\mathbf{x}_R, \mathbf{x}_A, t - t') dt', \quad (17)$$

for \mathbf{x}_A and \mathbf{x}'_A at \mathbb{S}_A . Hence, $f_{1,d}^+(\mathbf{x}_R, \mathbf{x}_A, t)$ is the (in practice band-limited) inverse of $T_d(\mathbf{x}_A, \mathbf{x}_R, t)$. When a macro model of the medium between \mathbb{S}_0 and \mathbb{S}_A is available, T_d can be derived from this model and inverted to obtain $f_{1,d}^+$. For convenience, this inversion is often approximated by time-reversal, according to $f_{1,d}^+(\mathbf{x}_R, \mathbf{x}_A, t) \approx T_d(\mathbf{x}_A, \mathbf{x}_R, -t)$. The Marchenko scheme appears to be quite robust with respect to amplitude and timing errors in the direct arrival of the focusing function (Broggini et al., 2014; Wapenaar et al., 2014). Nevertheless, for horizontally layered media the amplitude of the direct arrival can be corrected, using the principle of energy conservation (Mildner et al., 2019). For highly complex media it can be advantageous to account for wavefield complexity in the initial estimate of the focusing function (Vasconcelos et al., 2015; Vasconcelos and Sripanich, 2019). In the section ‘‘Marchenko multiple elimination’’ we discuss methods that are independent of the direct arrival of the focusing function.

The essential expressions for the retrieval of the focusing functions, i.e., the Marchenko equations and the Marchenko scheme in compact operator form, are summarized in Box 1. This box also shows the main expressions for the other methods discussed in the current section ‘‘Marchenko redatuming and imaging’’.

Retrieval of Green’s functions (source redatuming)

Once the focusing functions have been found, the next step is the retrieval of the Green’s functions. We define time windows $\Psi_a(\mathbf{x}_R, \mathbf{x}_A, t)$ and $\Psi_b(\mathbf{x}_R, \mathbf{x}_A, t)$ via

$$\Psi_{a,b}(\mathbf{x}_R, \mathbf{x}_A, t) = 1 - \Theta_{a,b}(\mathbf{x}_R, \mathbf{x}_A, t). \quad (18)$$

Note that the windows $\Psi_{a,b}(\mathbf{x}_R, \mathbf{x}_A, t)$ are complementary to $\Theta_{a,b}(\mathbf{x}_R, \mathbf{x}_A, t)$, defined in equations 8 and 9. Hence, they pass the Green’s functions and suppress the focusing functions, except $f_{1,d}^+$, see Figure 2c. Application of $\Psi_b(\mathbf{x}_R, \mathbf{x}_A, t)$ to both sides of equation 4 thus gives

$$G^{-,+}(\mathbf{x}_R, \mathbf{x}_A, t) = \Psi_b \int_{\mathbb{S}_0} d\mathbf{x}_S \int_0^\infty R(\mathbf{x}_R, \mathbf{x}_S, t') f_1^+(\mathbf{x}_S, \mathbf{x}_A, t - t') dt'. \quad (19)$$

Similarly, applying $\Psi_a(\mathbf{x}_R, \mathbf{x}_A, t)$ to both sides of equation 5 yields

$$G^{-,-}(\mathbf{x}_R, \mathbf{x}_A, -t) + f_{1,d}^+(\mathbf{x}_R, \mathbf{x}_A, t) = \Psi_a \int_{\mathbb{S}_0} d\mathbf{x}_S \int_{-\infty}^0 R(\mathbf{x}_R, \mathbf{x}_S, -t') f_1^-(\mathbf{x}_S, \mathbf{x}_A, t - t') dt'. \quad (20)$$

We interpret these expressions as follows. The reflection response on the right-hand sides is the response to an actual source at \mathbf{x}_S , observed by an actual receiver at \mathbf{x}_R , both at the acquisition surface \mathbb{S}_0 . This is visualized in Figure 3a. The Green’s functions on the left-hand sides are responses to a virtual source for downgoing waves (equation 19) and upgoing waves (equation 20) at \mathbf{x}_A in the subsurface, observed by the actual receiver at \mathbf{x}_R at the surface. Hence, equations 19 and 20 accomplish source redatuming from \mathbf{x}_S at the acquisition surface \mathbb{S}_0 to virtual-source position \mathbf{x}_A in the subsurface. Figure 3b visualizes equation 19.

Equation 19 and Figure 3b resemble the virtual-source method proposed by Bakulin and Calvert (2006), except that in their formulation the actual receivers are situated in a horizontal borehole and, instead of using a Marchenko-derived focusing function, they use a windowed time-reversed response between sources at the surface and an actual receiver at \mathbf{x}_A in the borehole. Hence, when measurements are available in a borehole, their method enables the retrieval of the response to a virtual source at \mathbf{x}_A below a complex overburden. Note, however, that their method does not account for internal multiples.

In the compact operator notation, equations 19 and 20 for source redatuming become

$$G_{R,A}^{-,+} = \Psi_b R f_1^+, \quad (21)$$

$$G_{R,A}^{-,-*} = \Psi_a R^* f_1^- - f_{1,d}^+, \quad (22)$$

where the subscripts R and A on the left-hand sides refer to the actual receiver position \mathbf{x}_R at the surface \mathbb{S}_0 and the virtual-source position \mathbf{x}_A at the datum plane \mathbb{S}_A in the subsurface. In the following we discuss different methods to redatum also the receivers from the surface to a virtual-receiver position \mathbf{x}_B at \mathbb{S}_A .

Receiver redatuming by MDD

We define the reflection response at datum plane \mathbb{S}_A of the target below \mathbb{S}_A as $R_{\text{tar}}(\mathbf{x}_B, \mathbf{x}_A, t) = G^{-,+}(\mathbf{x}_B, \mathbf{x}_A, t)$, with \mathbf{x}_A and \mathbf{x}_B both at \mathbb{S}_A (subscript ‘tar’ stands for ‘target’). Note that, when $G^{-,+}(\mathbf{x}_B, \mathbf{x}_A, t)$ is defined in the actual medium, it not only contains the response of the medium below \mathbb{S}_A , but also multiples between reflectors below and above \mathbb{S}_A (the dashed rays in Figure 4a). We define a truncated medium, which is identical to the actual

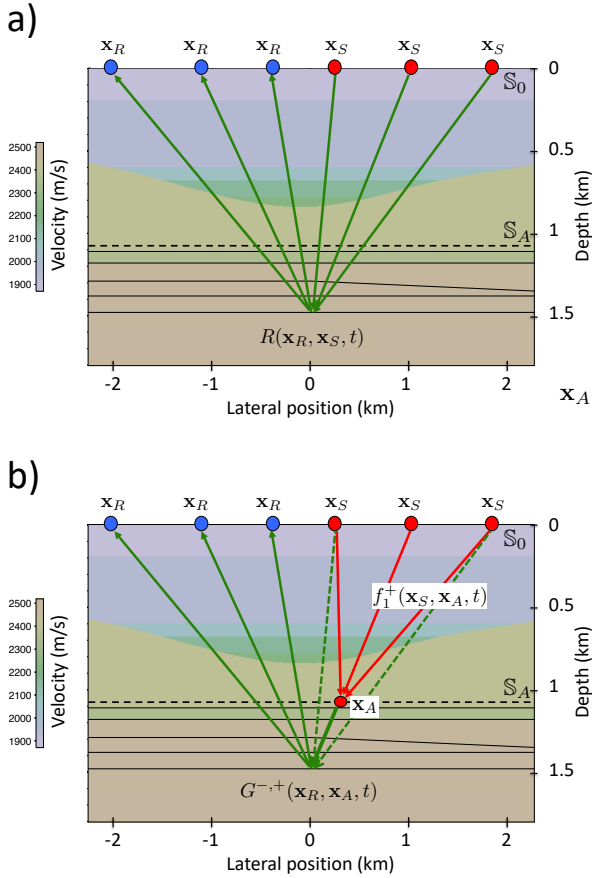


FIG. 3 (a) Reflection response at the surface. Only a few rays are shown, mainly to indicate in which direction a wave leaves a source and arrives at a receiver, but note that the reflection response includes all primary and internal multiple reflections. (b) Visualization of equation 19 (source redatuming). The red rays indicate the focusing function (shown in more detail in Figure 1a) and the solid green rays represent the Green's function (shown in more detail in Figure 2a).

medium below \mathbb{S}_A and reflection free above \mathbb{S}_A (note that this is complementary to the truncated medium in which the focusing functions are defined). We denote the reflection response at \mathbb{S}_A of this truncated medium as $\bar{R}_{\text{tar}}(\mathbf{x}_B, \mathbf{x}_A, t) = \bar{G}^{-,+}(\mathbf{x}_B, \mathbf{x}_A, t)$. Obviously this response does not contain the kind of multiples mentioned above (Figure 4b).

The target reflection response $\bar{R}_{\text{tar}}(\mathbf{x}_B, \mathbf{x}_A, t)$ and the virtual-source responses defined in equations 19 and 20 are mutually related via

$$G^{-,+}(\mathbf{x}_R, \mathbf{x}_A, t) = - \int_{\mathbb{S}_A} d\mathbf{x}_B \int_0^t G^{-,-}(\mathbf{x}_R, \mathbf{x}_B, t') \bar{R}_{\text{tar}}(\mathbf{x}_B, \mathbf{x}_A, t - t') dt' \quad (23)$$

(Wapenaar, 1996; Amundsen, 2001; Reinicke et al., 2020). This relation is visualized in Figure 4c. The finite time integration interval follows from the fact that

both quantities under the integral are causal functions of time. Equation 23 describes a multidimensional convolution, along time and space. Hence, resolving the target reflection response $\bar{R}_{\text{tar}}(\mathbf{x}_B, \mathbf{x}_A, t)$ from this equation is a multidimensional deconvolution (MDD) process, which redatums the receivers from \mathbb{S}_0 to \mathbb{S}_A . We thus obtain the redatumed reflection response $\bar{R}_{\text{tar}}(\mathbf{x}_B, \mathbf{x}_A, t)$, with its virtual source at \mathbf{x}_A and its virtual receiver at \mathbf{x}_B , both at \mathbb{S}_A . In principle all effects of the overburden, including its internal multiple reflections, are completely removed by the redatuming process. For a field data application we refer to Ravasi et al. (2016).

This MDD redatuming method resembles a process called rigorous redatuming, proposed by Mulder (2005), which also retrieves the target reflection response $\bar{R}_{\text{tar}}(\mathbf{x}_B, \mathbf{x}_A, t)$ from the reflection data at the surface. This method requires an accurate model of the medium between \mathbb{S}_0 and \mathbb{S}_A , explaining the primaries and the internal multiples. On the contrary, the Marchenko-based method only needs a macro model that explains the direct transmission response T_d between \mathbb{S}_0 and \mathbb{S}_A . The information needed to explain the internal multiples comes directly from the reflection response at the surface, see equation 16.

In the compact operator notation, equation 23 becomes

$$G_{R,A}^{-,+} = -G_{R,B}^{-,-} \bar{R}_{\text{tar}}. \quad (24)$$

In this notation, receiver redatuming by MDD is formally described by

$$\bar{R}_{\text{tar}} = -(G_{R,B}^{-,-})^{-1} G_{R,A}^{-,+}. \quad (25)$$

Note that $G_{R,A}^{-,+}$ and $G_{R,B}^{-,-}$ both depend linearly on $f_{1,d}^+$ (see equations 12, 16, 21 and 22). Hence, amplitude errors in $f_{1,d}^+$ are for the larger part cancelled in redatuming by MDD. This cancellation is complete when the medium is horizontally layered; it is approximate in a laterally varying medium. The redatumed response $\bar{R}_{\text{tar}}(\mathbf{x}_B, \mathbf{x}_A, t)$ is free of internal multiples related to the overburden and can be used as input for imaging the target zone, for example by standard reverse-time migration (RTM). Although this does not remove internal multiples in the target zone, it yields a significant improvement over applying RTM to the reflection response at the surface. We refer to Brogini et al. (2014) for numerical examples.

Instead of inverting $G_{R,B}^{-,-}$, the target response \bar{R}_{tar} can be resolved directly from equation 24 by recasting the problem in terms of linear operators, which avoids the stabilization of $(G_{R,B}^{-,-})^{-1}$ needed in equation 25 (Luiken and van Leeuwen, 2020).

The redatuming method we discuss in the next section is based on an explicit expression for R_{tar} and is therefore better equipped for practical applications.

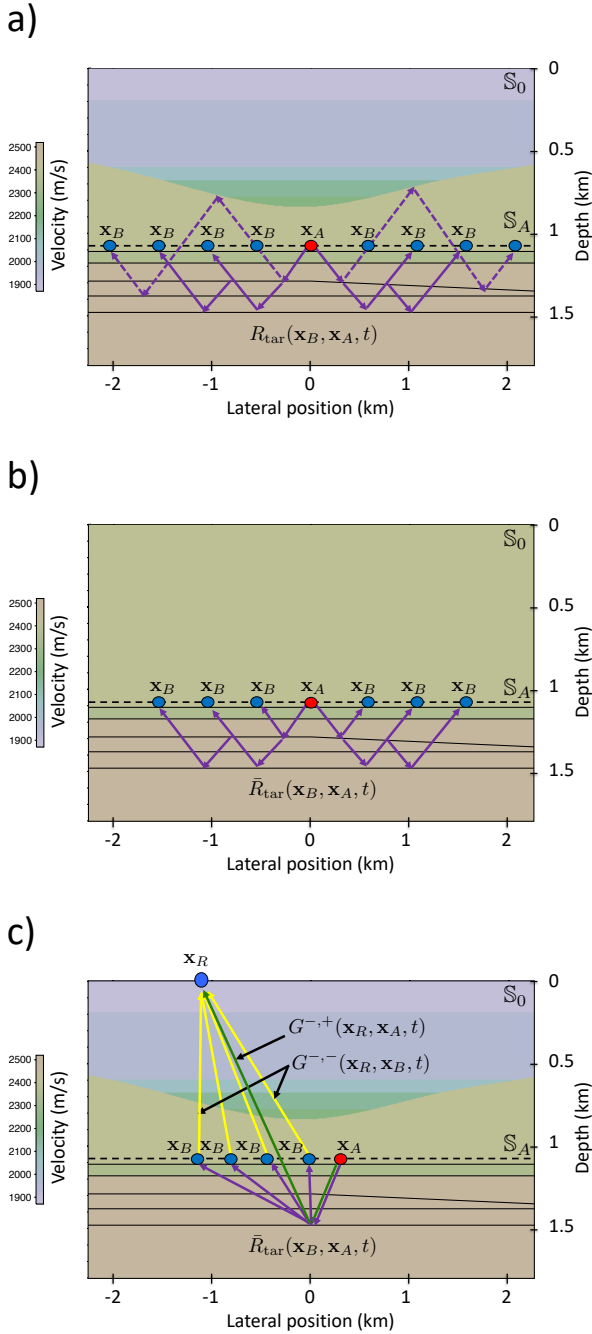


FIG. 4 (a) The reflection response $R_{\text{tar}}(\mathbf{x}_B, \mathbf{x}_A, t) = G^{-,+}(\mathbf{x}_B, \mathbf{x}_A, t)$ in the actual medium. (b) The reflection response $\bar{R}_{\text{tar}}(\mathbf{x}_B, \mathbf{x}_A, t) = \bar{G}^{-,+}(\mathbf{x}_B, \mathbf{x}_A, t)$ in the truncated medium. (c) Visualization of equation 23. The Green's functions are shown in more detail in Figure 2a and the reflection response $\bar{R}_{\text{tar}}(\mathbf{x}_B, \mathbf{x}_A, t)$ in Figure 4b.

Source and receiver redatuming by double focusing

Consider again equation 19, which describes source redatuming. Receiver redatuming can be formulated

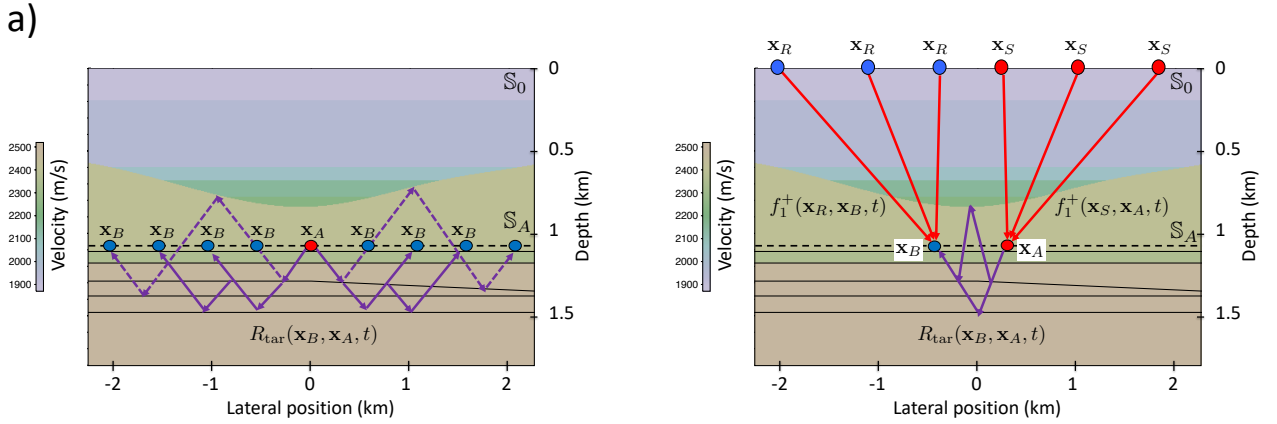


FIG. 5 Visualization of equation 26 (receiver redatuming), applied to the output of 19 (source redatuming, see Figure 3b). The combination of these two processes (captured by equation 28) is called redatuming by double focusing. The red rays indicate the focusing function (shown in more detail in Figure 1a) and the purple rays represent the redatumed reflection response at \mathbb{S}_A in the actual medium (shown in more detail in Figure 4a).

in a similar way, according to

$$R_{\text{tar}}(\mathbf{x}_B, \mathbf{x}_A, t) = \int_{\mathbb{S}_0} d\mathbf{x}_R \int_0^\infty f_1^+(\mathbf{x}_R, \mathbf{x}_B, t - t') G^{-,+}(\mathbf{x}_R, \mathbf{x}_A, t') dt' \quad (26)$$

(van der Neut et al., 2017; Wapenaar et al., 2019), where $R_{\text{tar}}(\mathbf{x}_B, \mathbf{x}_A, t) = G^{-,+}(\mathbf{x}_B, \mathbf{x}_A, t)$, with \mathbf{x}_A and \mathbf{x}_B both at \mathbb{S}_A (see the Appendix for details). The Green's function under the integral, $G^{-,+}(\mathbf{x}_R, \mathbf{x}_A, t)$, is the output of equation 19, which describes how the actual sources at \mathbf{x}_S are focused onto the virtual source at \mathbf{x}_A , see Figure 3b. Similarly, equation 26 describes how the actual receivers at \mathbf{x}_R are focused onto the virtual receiver at \mathbf{x}_B , see Figure 5. Hence, the combination of equations 19 and 26 can be seen as a double focusing process, which is also clearly seen in Figure 5. Note that the redatumed response $\bar{R}_{\text{tar}}(\mathbf{x}_B, \mathbf{x}_A, t)$ is defined in the actual medium, hence, apart from the response of the target below and above \mathbb{S}_A . This can be seen as a disadvantage compared with redatuming by MDD, which delivers the response $\bar{R}_{\text{tar}}(\mathbf{x}_B, \mathbf{x}_A, t)$ in the truncated medium (Figure 4b). However, the fact that redatuming by double focusing does not require inversion often outweighs this disadvantage.

In the compact operator notation, equation 26 becomes

$$R_{\text{tar}} = f_1^{+t} G_{R,A}^{-,+}, \quad (27)$$

where superscript t denotes operator transposition (the operator f_1^{+t} acts on the receiver coordinate in-

stead of on the source coordinate). Combined with equation 21 this gives

$$R_{\text{tar}} = f_1^{+t} \Psi_b R f_1^+. \quad (28)$$

We call this source and receiver redatuming by double focusing. Note the similarity with the classical redatuming scheme (Berkhout, 1982; Berryhill, 1984; Berkhout and Wapenaar, 1993), which in the compact operator notation reads

$$R_{\text{tar}} \approx f_{1,d}^{+t} R f_{1,d}^+. \quad (29)$$

Recall that $f_{1,d}^+$ is the direct contribution of focusing operator f_1^+ , see Figures 1a and 1b. Hence, equation 29 only accounts for primary waves. Operator f_1^+ in equation 28, on the other hand, accounts for primaries and internal multiple reflections in the overburden (the region between \mathbb{S}_0 and \mathbb{S}_A).

Upon substitution of equation 16 into equation 28, we obtain

$$R_{\text{tar}} = f_{1,d}^{+t} \Psi_b R f_{1,d}^+ - (-f_{1,d}^{+t} \Psi_b R \Omega f_{1,d}^+) - (-\Omega f_{1,d}^+)^t \Psi_b R f_{1,d}^+ - (-\Omega f_{1,d}^+)^t \Psi_b R \Omega f_{1,d}^+ + \dots, \quad (30)$$

with $\Omega = \Theta_a R^* \Theta_b R$ (Staring et al., 2018). The first term on the right-hand side stands for primary redatuming. Each of the subsequent terms in this expansion accounts for the prediction and subtraction of a specific order of internal multiple reflections. In theory the scheme converges, so when the reflection response is accurately known there is no need to apply this subtraction adaptively. However, in practice there will be imperfections in R . The expansion in equation 30 opens the possibility to implement the redatuming scheme in an adaptive way, by applying weighting factors or adaptive filters, which will make Marchenko redatuming more robust (van der Neut et al., 2015c). We emphasize that an adaptive implementation is only needed to compensate for imperfections in the reflection response and for attenuation but not for limitations of the theory. Field data applications of this method (2D and 3D) are presented by Staring et al. (2018) and Staring and Wapenaar (2020).

Once the data have been redatumed, they can be used as input for imaging of the target zone below the redatuming level \mathbb{S}_A . In principle any migration scheme can be used for this. This will lead to an image of the target zone, free of artefacts related to internal multiples in the overburden. However, internal multiples related to the target and multiples between reflectors below and above \mathbb{S}_A may still lead to artefacts. In the field data applications mentioned above, these multiples do not play a significant role. Nevertheless, there is a way to further reduce the effects of these remaining multiples. Instead of redatuming to a single depth level, redatuming can be carried out to multiple depth levels, followed by migration of the

regions between these depth levels. Ultimately, redatuming can be carried out to all depth levels where an image is required, followed by selecting the zero-offset component at zero time of the redatumed data, i.e., $R_{\text{tar}}(\mathbf{x}_B, \mathbf{x}_B, t = 0)$. This function, for all \mathbf{x}_B in the region of interest, forms an image $r_{\text{im}}(\mathbf{x}_B)$ of the local reflection coefficient, free of artefacts related to all multiple reflections. Since in the latter approach only the $t = 0$ component of R_{tar} is selected, it suffices to replace f_1^{+t} in equation 28 by $f_{1,d}^{+t}$ and skip the window function Ψ_b . Hence, the imaging scheme thus becomes

$$r_{\text{im}} = (f_{1,d}^{+t} R f_1^+)_{\mathbf{x}_B = \mathbf{x}_A, t=0}, \quad (31)$$

where r_{im} stands for $r_{\text{im}}(\mathbf{x}_B)$.

Virtual seismology

The redatumed response $R_{\text{tar}}(\mathbf{x}_B, \mathbf{x}_A, t)$, obtained by the double focusing method (equation 28), stands for the Green's function $G^{-,+}(\mathbf{x}_B, \mathbf{x}_A, t)$. This is the response to a source for downgoing waves at \mathbf{x}_A , observed by a receiver for upgoing waves at \mathbf{x}_B , with \mathbf{x}_A and \mathbf{x}_B both at the same boundary \mathbb{S}_A in the subsurface. Here we generalise equation 28 for the situation where \mathbf{x}_A and \mathbf{x}_B do not lie on the same horizontal boundary and we discuss similar expressions for $G^{+,+}(\mathbf{x}_B, \mathbf{x}_A, t)$, $G^{-,-}(\mathbf{x}_B, \mathbf{x}_A, t)$ and $G^{+,-}(\mathbf{x}_B, \mathbf{x}_A, t)$.

For \mathbf{x}_A and \mathbf{x}_B at different depth levels, equation 26 for receiver redatuming is generalized to

$$G^{-,+}(\mathbf{x}_B, \mathbf{x}_A, t) + \theta(x_{3,B} - x_{3,A}) f_1^-(\mathbf{x}_A, \mathbf{x}_B, t) \quad (32) \\ = \int_{\mathbb{S}_0} d\mathbf{x}_R \int_0^\infty f_1^+(\mathbf{x}_R, \mathbf{x}_B, t - t') G^{-,+}(\mathbf{x}_R, \mathbf{x}_A, t') dt',$$

see the Appendix for details. Here the Green's function under the integral, $G^{-,+}(\mathbf{x}_R, \mathbf{x}_A, t)$, is the result of source redatuming, according to equation 19. In the compact operator notation, equation 32 becomes

$$G_{B,A}^{-,+} + \theta_{B,A} f_1^- = f_1^{+t} G_{R,A}^{-,+}, \quad (33)$$

where $G_{R,A}^{-,+}$ is obtained from equation 21 and $\theta_{B,A}$ is the compact notation for the Heaviside function in equation 32. In a similar way we obtain (see Appendix)

$$G_{B,A}^{+,+*} - \theta_{B,A} f_1^+ = -f_1^{-t} G_{R,A}^{-,+*}, \quad (34)$$

$$G_{B,A}^{-,-} - \theta_{B,A} f_1^+ = f_1^{+t} G_{R,A}^{-,-}, \quad (35)$$

$$G_{B,A}^{+,-*} + \theta_{B,A} f_1^- = -f_1^{-t} G_{R,A}^{-,-*}, \quad (36)$$

where $G_{R,A}^{-,-*}$ is obtained from equation 22. Equations 33 – 36 show how the four components of the decomposed Green's function between \mathbf{x}_A and \mathbf{x}_B can

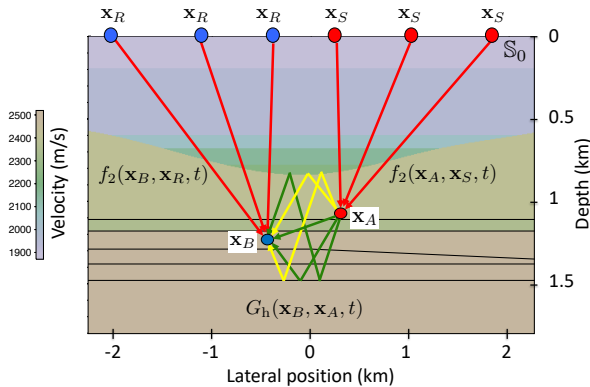


FIG. 6 Visualization of equation 38 (virtual seismology). The retrieved homogeneous Green’s function $G_h(\mathbf{x}_B, \mathbf{x}_A, t)$ consists of $G_{B,A}^{+,+} + G_{B,A}^{-,+}$ (green rays), $-G_{B,A}^{+,-} - G_{B,A}^{-,-}$ (yellow rays) and their time-reversals.

be separately obtained. We can suppress the terms $\theta_{B,A} f_1^\pm$ on the left-hand sides by combining the four components as follows

$$G_{B,A}^{+,+*} + G_{B,A}^{-,+} - G_{B,A}^{+,-*} - G_{B,A}^{-,-} = \quad (37)$$

$$f_1^{+t}(G_{R,A}^{-,+} - G_{R,A}^{-,-}) - f_1^{-t}(G_{R,A}^{-,+*} - G_{R,A}^{-,-*}).$$

Adding to both sides its time-reversal and substituting equations 21 and 22 yields

$$G_{B,A} + G_{B,A}^* = f_2^t(\Psi R f_2 + f_{1,d}^{+*}) + \{f_2^t(\Psi R f_2 + f_{1,d}^{+*})\}^* \quad (38)$$

(van der Neut et al., 2017; Wapenaar et al., 2017), with Green’s function $G_{B,A}$ defined as

$$G_{B,A} = G_{B,A}^{+,+} + G_{B,A}^{-,+} - G_{B,A}^{+,-} - G_{B,A}^{-,-} \quad (39)$$

and focusing function f_2 as

$$f_2 = f_1^+ - f_1^{+*}. \quad (40)$$

In the section ‘Transmission-loss compensated primary retrieval’ we discuss the physical meaning of f_2 in more detail; here we simply define it as a specific combination of f_1^+ and f_1^- , formulated by equation 40. The left-hand side of equation 38 is the so-called homogeneous Green’s function $G_h(\mathbf{x}_B, \mathbf{x}_A, t) = G(\mathbf{x}_B, \mathbf{x}_A, t) + G(\mathbf{x}_B, \mathbf{x}_A, -t)$ between a source at \mathbf{x}_A and a receiver at \mathbf{x}_B , see Figure 6 (actually it is the power-flux normalized homogeneous Green’s function; the pressure-normalized version is obtained by applying composition operators $\mathcal{L}_1(\mathbf{x}_A)$ and $\mathcal{L}_1(\mathbf{x}_B)$ at the source- and receiver sides (Wapenaar et al., 2014)). Equation 38 is the basis for ‘virtual seismology’. This term refers to the methodology for retrieving virtual seismic responses between sources and receivers in the subsurface from reflection data at the surface, prop-

erly accounting for internal multiples. This methodology can be used, for example, to monitor the response to actual induced seismic sources with virtual receivers in the subsurface or to forecast the response to possible future induced seismic sources. This is explained in more detail and illustrated with numerical and field data examples by Brackenhoff et al. (2019a,b).

Plane-wave redatuming

Taner (1976) and Schultz and Claerbout (1978) designed a method to synthesize the reflection response to a plane wave at the surface. Rietveld et al. (1992) modified this approach to synthesize plane-wave sources in the subsurface. An advantage is that an image of a target zone can be obtained by migrating only a limited number of plane-wave responses (with different illumination angles) instead of a relatively large number of point-source responses. The approach of Rietveld et al. (1992) employs the primary transmission response of the overburden to synthesize the plane-wave sources, hence internal multiples are not taken into account. Meles et al. (2018) propose to use the focusing functions obtained with the Marchenko method to synthesize virtual plane-wave sources in the subsurface. With this method, plane-wave responses are obtained that are free of artefacts related to the internal multiples of the overburden. Here we briefly discuss this method.

We start by defining the 3D plane-wave focusing function $f_1^\pm(\mathbf{x}, \mathbf{p}_A, t)$ in the truncated medium (which is reflection free below \mathbb{S}_A) as the integral of focusing functions $f_1^\pm(\mathbf{x}, \mathbf{x}_A, t)$ over all possible focal points \mathbf{x}_A at \mathbb{S}_A , according to

$$\tilde{f}_1^\pm(\mathbf{x}, \mathbf{p}_A, t) = \int_{\mathbb{S}_A} f_1^\pm(\mathbf{x}, \mathbf{x}_A, t - \mathbf{p} \cdot \mathbf{x}_{H,A}) d\mathbf{x}_A, \quad (41)$$

with $\mathbf{p} = (p_1, p_2)$ and \mathbf{p}_A being a short notation for $(\mathbf{p}, x_{3,A})$. Here p_1 and p_2 are the horizontal rayparameters. For a laterally constant velocity c at \mathbb{S}_A , the rayparameters are related to the dip angle α and the azimuth angle β via $p_1 = c^{-1} \sin \alpha \cos \beta$ and $p_2 = c^{-1} \sin \alpha \sin \beta$; for 2D situations, vector \mathbf{p} reduces to $\mathbf{p} = p_1$, with $p_1 = c^{-1} \sin \alpha$. The following derivation does not rely on a laterally constant velocity assumption.

When $\mathbf{p} = \mathbf{0}$, equation 41 integrates the focusing functions of Figure 1 without a time delay, hence, $\tilde{f}_1^+(\mathbf{x}, \mathbf{0}, x_{3,A}, t)$ focuses as a horizontal plane wave at \mathbb{S}_A and $t = 0$ and continues as a horizontal downgoing plane wave into the half-space below \mathbb{S}_A . For arbitrary \mathbf{p} , $\tilde{f}_1^+(\mathbf{x}, \mathbf{p}_A, t)$ focuses as a dipping plane wave at \mathbb{S}_A , according to

$$\tilde{f}_1^+(\mathbf{x}'_A, \mathbf{p}_A, t) = \delta(t - \mathbf{p} \cdot \mathbf{x}'_{H,A}), \quad (42)$$

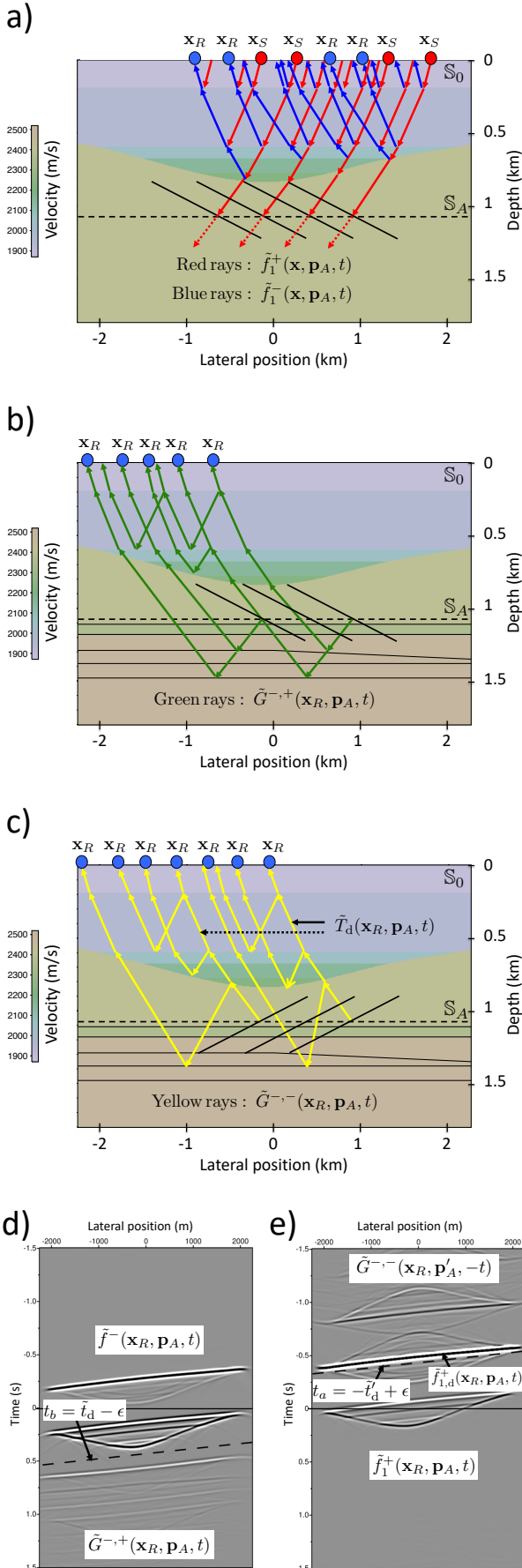


FIG. 7 (a) Plane-wave focusing functions in the truncated medium (here shown for a negative value of p_1 and $p_2 = 0$). (b,c) Plane-wave Green's functions in the actual medium. (d) The left-hand side of equation 44 (fixed \mathbf{p}_A , variable \mathbf{x}_R). (e) The left-hand side of equation 45.

for \mathbf{x}'_A at \mathbb{S}_A (which follows from substituting equation 2 into 41). Note that, whereas the original focusing functions focus in space and time (equation 2), the plane-wave focusing function focuses in time only (equation 42). The upgoing focusing function $\tilde{f}_1^-(\mathbf{x}_R, \mathbf{p}_A, t)$ is the response of the truncated medium to $\tilde{f}_1^+(\mathbf{x}_S, \mathbf{p}_A, t)$, observed at \mathbf{x}_R at \mathbb{S}_0 . Both the downgoing and upgoing plane-wave functions are visualized in Figure 7a.

We define the plane-wave Green's functions in the actual medium in a similar way, hence

$$\tilde{G}^{-,\pm}(\mathbf{x}_R, \mathbf{p}_A, t) = \int_{\mathbb{S}_A} G^{-,\pm}(\mathbf{x}_R, \mathbf{x}_A, t - \mathbf{p} \cdot \mathbf{x}_{H,A}) d\mathbf{x}_A. \quad (43)$$

Here $\tilde{G}^{-,+}(\mathbf{x}_R, \mathbf{p}_A, t)$ is interpreted as the response to a source for dipping downgoing plane waves at \mathbb{S}_A , observed by receivers for upgoing waves at \mathbf{x}_R at \mathbb{S}_0 , see Figure 7b. Similarly, $\tilde{G}^{-,-}(\mathbf{x}_R, \mathbf{p}_A, t)$ is interpreted as the response to a source for dipping upgoing plane waves at \mathbb{S}_A , see Figure 7c.

Applying similar integrations to the left- and right-hand sides of equations 4 and 5, we obtain

$$\tilde{G}^{-,+}(\mathbf{x}_R, \mathbf{p}_A, t) + \tilde{f}_1^-(\mathbf{x}_R, \mathbf{p}_A, t) = \int_{\mathbb{S}_0} d\mathbf{x}_S \int_0^\infty R(\mathbf{x}_R, \mathbf{x}_S, t') \tilde{f}_1^+(\mathbf{x}_S, \mathbf{p}_A, t - t') dt' \quad (44)$$

and

$$\tilde{G}^{-,-}(\mathbf{x}_R, \mathbf{p}'_A, -t) + \tilde{f}_1^+(\mathbf{x}_R, \mathbf{p}_A, t) = \int_{\mathbb{S}_0} d\mathbf{x}_S \int_{-\infty}^0 R(\mathbf{x}_R, \mathbf{x}_S, -t') \tilde{f}_1^-(\mathbf{x}_S, \mathbf{p}_A, t - t') dt', \quad (45)$$

where \mathbf{p}'_A stands for $(-\mathbf{p}, x_{3,A})$. Equation 44 can be interpreted in a similar way as equation 4. The right-hand side quantifies the response of the actual medium to the downgoing focusing function $\tilde{f}_1^+(\mathbf{x}_S, \mathbf{p}_A, t)$. In Figure 7a it is seen that this gives the upgoing focusing function $\tilde{f}_1^-(\mathbf{x}_R, \mathbf{p}_A, t)$ at \mathbb{S}_0 and a focused plane wave at \mathbb{S}_A , which acts as a virtual source for downgoing plane waves. Figure 7b shows that the response to this virtual source is the Green's function $\tilde{G}^{-,+}(\mathbf{x}_R, \mathbf{p}_A, t)$ on the left-hand side of equation 44. Similarly, the right-hand side of equation 45 quantifies the response of the time-reversed actual medium to the upgoing focusing function $\tilde{f}_1^-(\mathbf{x}_S, \mathbf{p}_A, t)$. The functions on the left-hand sides of equations 44 and 45, convolved with a wavelet, are shown in grey-level display in Figures 7d and 7e, respectively.

To retrieve the plane-wave focusing functions from the reflection response R , we could first retrieve the functions $f_1^\pm(\mathbf{x}, \mathbf{x}_A, t)$ for all \mathbf{x}_A at \mathbb{S}_A and subsequently obtain $\tilde{f}_1^\pm(\mathbf{x}, \mathbf{p}_A, t)$ by evaluating equation 41. However, it is computationally much more efficient to retrieve these functions directly in the plane-wave

domain, by suppressing the plane-wave Green's functions from equations 44 and 45 and solving the remaining system of equations for the plane-wave focusing functions. To determine the window functions for suppressing the Green's functions, we need to know the first possible arrival of $\tilde{G}^{-,+}(\mathbf{x}_R, \mathbf{p}_A, t)$ and the last arrival of the time reversed function $\tilde{G}^{-,-}(\mathbf{x}_R, \mathbf{p}'_A, -t)$. The first possible arrival of $\tilde{G}^{-,+}(\mathbf{x}_R, \mathbf{p}_A, t)$ (which would occur when there would be a reflector just below \mathbb{S}_A) is obtained by substituting equation 6 into equation 43, hence

$$\{\tilde{G}^{-,+}(\mathbf{x}_R, \mathbf{p}_A, t)\}_{\text{first}} \propto \int_{\mathbb{S}_A} T_d(\mathbf{x}_R, \mathbf{x}_A, t - \mathbf{p} \cdot \mathbf{x}_{H,A}) d\mathbf{x}_A = \tilde{T}_d(\mathbf{x}_R, \mathbf{p}_A, t). \quad (46)$$

Here $\tilde{T}_d(\mathbf{x}_R, \mathbf{p}_A, t)$ is the direct arrival of the transmission response to a dipping plane wave, emitted upward from \mathbb{S}_A with rayparameter \mathbf{p} , observed by a receiver at \mathbf{x}_R (this is also the direct arrival of $\tilde{G}^{-,-}(\mathbf{x}_R, \mathbf{p}_A, t)$, see Figure 7c). We denote the arrival time of this direct transmission response as $\tilde{t}_d(\mathbf{x}_R, \mathbf{p}_A)$. Hence, $\tilde{G}^{-,+}(\mathbf{x}_R, \mathbf{p}_A, t)$ can be suppressed from equation 44 by a time window that removes everything beyond $t = t_b = \tilde{t}_d(\mathbf{x}_R, \mathbf{p}_A) - \epsilon$ (the dashed line in Figure 7d, indicated by $t_b = \tilde{t}_d - \epsilon$). The last arrival of the time-reversed Green's function $\tilde{G}^{-,-}(\mathbf{x}_R, \mathbf{p}'_A, -t)$ is obtained by substituting equation 7 into equation 43, hence

$$\{\tilde{G}^{-,-}(\mathbf{x}_R, \mathbf{p}'_A, -t)\}_{\text{last}} = -\tilde{T}_d(\mathbf{x}_R, \mathbf{p}'_A, -t). \quad (47)$$

The arrival time of this event is $-\tilde{t}_d(\mathbf{x}_R, \mathbf{p}'_A)$. Hence, $\tilde{G}^{-,-}(\mathbf{x}_R, \mathbf{p}'_A, -t)$ can be suppressed from equation 45 by a time window that removes everything before $t = t_a = -\tilde{t}_d(\mathbf{x}_R, \mathbf{p}'_A) + \epsilon$ (the dashed line in Figure 7e, indicated by $t_a = -\tilde{t}'_d + \epsilon$). We define two time windows as

$$\tilde{\Theta}_a(\mathbf{x}_R, \mathbf{p}_A, t) = \theta(t - t_a) = \theta(t + \tilde{t}'_d - \epsilon), \quad (48)$$

$$\tilde{\Theta}_b(\mathbf{x}_R, \mathbf{p}_A, t) = \theta(t_b - t) = \theta(\tilde{t}_d - \epsilon - t). \quad (49)$$

These windows suppress the Green's functions and pass the focusing functions \tilde{f}_1^+ and \tilde{f}_1^- , except the direct plane-wave arrival $\tilde{f}_{1,d}^+(\mathbf{x}_R, \mathbf{p}_A, t)$, which coincides with the last arrival of $\tilde{G}^{-,-}(\mathbf{x}_R, \mathbf{p}'_A, -t)$, see Figure 7e.

Application of the windows $\tilde{\Theta}_{a,b}(\mathbf{x}_R, \mathbf{p}_A, t)$ to both sides of equations 44 and 45 gives, in the compact operator notation,

$$\tilde{f}_1^- = \tilde{\Theta}_b R \tilde{f}_1^+, \quad (50)$$

$$\tilde{f}_1^+ = \tilde{\Theta}_a R^* \tilde{f}_1^- + \tilde{f}_{1,d}^+. \quad (51)$$

These are the Marchenko equations for the plane-wave focusing functions. They can be solved, analogous to

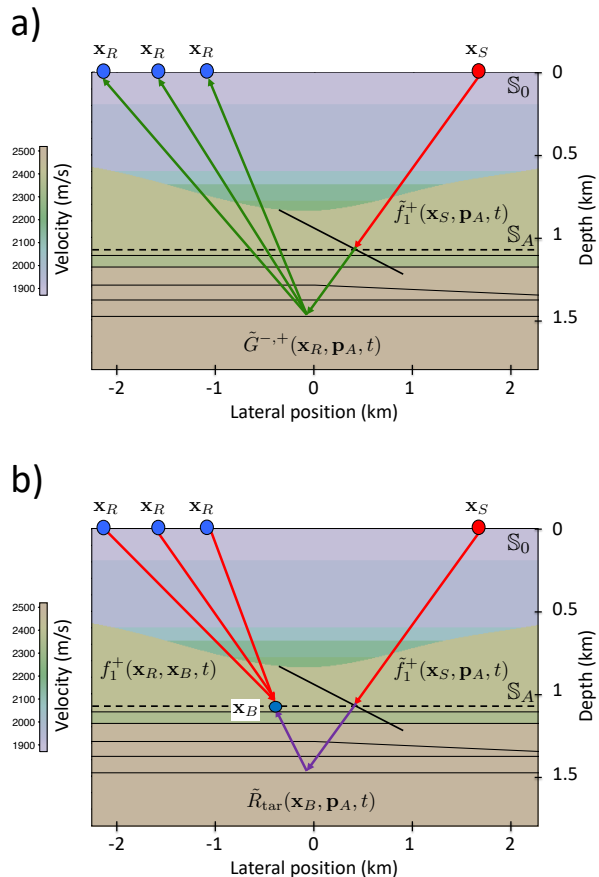


FIG. 8 (a) Visualization of equation 53 (plane-wave source redatuming). The red ray indicates the plane-wave focusing function (shown in more detail in Figure 7a) and the green rays represent the plane-wave Green's function (shown in more detail in Figure 7b). (b) Visualization of equation 55. The focusing function $f_1^+(\mathbf{x}_R, \mathbf{x}_B, t)$ is shown in more detail in Figure 1a. The purple rays represent the redatumed plane-wave reflection response at \mathbb{S}_A in the actual medium.

equation 16, by

$$\tilde{f}_1^+ = \sum_{k=0}^K \{\tilde{\Theta}_a R^* \tilde{\Theta}_b R\}^k \tilde{f}_{1,d}^+. \quad (52)$$

The next step is the retrieval of the plane-wave Green's functions. We define complementary time windows as $\tilde{\Psi}_{a,b}(\mathbf{x}_R, \mathbf{p}_A, t) = 1 - \tilde{\Theta}_{a,b}(\mathbf{x}_R, \mathbf{p}_A, t)$. Application of these windows to both sides of equations 44 and 45 gives, in the compact operator notation,

$$\tilde{G}_{R,\mathbf{p}_A}^{-,+} = \tilde{\Psi}_b R \tilde{f}_1^+, \quad (53)$$

$$\tilde{G}_{R,\mathbf{p}'_A}^{-,-*} = \tilde{\Psi}_a R^* \tilde{f}_1^- - \tilde{f}_{1,d}^+, \quad (54)$$

where the subscripts on the left-hand sides refer to the position of the actual receiver and the rayparameter of the virtual plane-wave source.

The interpretation of equations 53 and 54 is that

they accomplish source redatuming from \mathbf{x}_S at the acquisition surface \mathbb{S}_0 to a virtual plane wave source at the datum plane \mathbb{S}_A in the subsurface. Figure 8a visualizes equation 53.

Analogous to equations 27 and 28, the receivers can now be redatumed from \mathbf{x}_R at the surface \mathbb{S}_0 to a virtual receiver at \mathbf{x}_B at \mathbb{S}_A , according to

$$\begin{aligned}\tilde{R}_{\text{tar}} &= f_1^{+t} \tilde{G}_{R, \mathbf{p}_A}^{-, +} \\ &= f_1^{+t} \tilde{\Psi}_b R \tilde{f}_1^+, \end{aligned} \quad (55)$$

where \tilde{R}_{tar} stands for the target reflection response $\tilde{R}_{\text{tar}}(\mathbf{x}_B, \mathbf{p}_A, t) = G^{-, +}(\mathbf{x}_B, \mathbf{p}_A, t)$, see Figure 8b. It is the response to a virtual downgoing plane-wave source at \mathbb{S}_A with rayparameter \mathbf{p} , observed by a virtual receiver for upgoing waves at \mathbf{x}_B . Note that the Marchenko method needs to be applied for each virtual receiver of interest. Hence, the computational advantage of plane-wave source-redatuming, which is typically limited to a small number of rayparameters, quickly diminishes when many virtual receiver positions are chosen. However, if we combine redatuming with imaging, we can replace the focusing function f_1^{+t} by its direct arrival $f_{1,d}^{+t}$ and skip the window function $\tilde{\Psi}_b$, similar as in imaging by double focusing (equation 31), hence

$$\tilde{r}_{\text{im}} = (f_{1,d}^{+t} R \tilde{f}_1^+)_{t=\mathbf{p} \cdot \mathbf{x}_{H,B}}, \quad (56)$$

where \tilde{r}_{im} stands for the angle-dependent local reflection coefficient $\tilde{r}_{\text{im}}(\mathbf{x}_B, \mathbf{p}_A)$ for all \mathbf{x}_B in the region of interest. Note that the imaging condition $t = \mathbf{p} \cdot \mathbf{x}_{H,B}$ (instead of $t = 0$) accounts for the fact that the virtual plane-wave source at depth $x_{3,A}$ is dipping when $\mathbf{p} \neq \mathbf{0}$. Using equation 56 as the basis for redatuming and imaging, the Marchenko method is only needed to retrieve the plane-wave focusing function \tilde{f}_1^+ for a limited number of rayparameters at each imaging depth. This implies a significant efficiency gain in comparison with redatuming and imaging based on equation 31, particularly for 3D applications. Meles et al. (2018) discuss applications of plane-wave redatuming and imaging to 2D numerically modeled data.

Box 1:
Marchenko redatuming and imaging

Equations for focusing functions
(Figures 1 and 2)

$$\begin{aligned} f_1^- &= \Theta_b R f_1^+ \\ f_1^+ &= \Theta_a R^* f_1^- + f_{1,d}^+ \end{aligned}$$

Retrieval of focusing functions

$$f_1^+ = \sum_{k=0}^K \{\Theta_a R^* \Theta_b R\}^k f_{1,d}^+$$

Retrieval of Green's functions =
Source redatuming (Figures 2 and 3)

$$\begin{aligned} G_{R,A}^{-,+} &= \Psi_b R f_1^+ \\ G_{R,A}^{-,*} &= \Psi_a R^* f_1^- - f_{1,d}^+ \end{aligned}$$

Receiver redatuming by MDD
(Figure 4)

$$\bar{R}_{\text{tar}} = -(G_{R,B}^{-,-})^{-1} G_{R,A}^{-,+}$$

Source and receiver redatuming by double focusing (Figure 5)

$$R_{\text{tar}} = f_1^{+t} \Psi_b R f_1^+$$

Redatuming and imaging

$$r_{\text{im}} = (f_{1,d}^{+t} R f_1^+)_{\mathbf{x}_B = \mathbf{x}_A, t=0}$$

Virtual seismology (Figure 6)

$$\begin{aligned} G_{B,A} + G_{B,A}^* &= f_2^t (\Psi R f_2 + f_{1,d}^{+*}) \\ &+ \{f_2^t (\Psi R f_2 + f_{1,d}^{+*})\}^* \end{aligned}$$

Retrieval of plane-wave focusing functions

$$\begin{aligned} \tilde{f}_1^+ &= \sum_{k=0}^K \{\tilde{\Theta}_a R^* \tilde{\Theta}_b R\}^k \tilde{f}_{1,d}^+ \\ \tilde{f}_1^- &= \tilde{\Theta}_b R \tilde{f}_1^+ \end{aligned}$$

Retrieval of plane-wave Green's functions =
Plane-wave source redatuming (Figure 7)

$$\begin{aligned} \tilde{G}_{R,\mathbf{p}_A}^{-,+} &= \tilde{\Psi}_b R \tilde{f}_1^+ \\ \tilde{G}_{R,\mathbf{p}'_A}^{-,*} &= \tilde{\Psi}_a R^* \tilde{f}_1^- - \tilde{f}_{1,d}^+ \end{aligned}$$

Plane-wave redatuming by double focusing
(Figure 8)

$$\tilde{R}_{\text{tar}} = f_1^{+t} \tilde{\Psi}_b R \tilde{f}_1^+$$

Plane-wave redatuming and imaging

$$\tilde{r}_{\text{im}} = (f_{1,d}^{+t} R \tilde{f}_1^+)_{t=\mathbf{p} \cdot \mathbf{x}_{H,B}}$$

Box 2:
Marchenko multiple elimination

Equations for extrapolated focusing functions
(Figure 10)

$$\begin{aligned} v^- &= f_1^- T_d = \Theta_b^v R v^+ \\ v^+ &= f_1^+ T_d = \Theta_a^v R^* v^- + \delta \end{aligned}$$

Retrieval of extrapolated focusing functions

$$v^+ = \sum_{k=0}^K \{\Theta_a^v R^* \Theta_b^v R\}^k \delta$$

Retrieval of extrapolated Green's functions =
Source-side dereverberation (Figures 9 and 10)

$$\begin{aligned} U_{R,S'}^{-,+} &= G_{R,A}^{-,+} T_d = \Psi_b^v R v^+ \\ U_{R,S'}^{-,*} &= G_{R,A}^{-,*} T_d = \Psi_a^v R^* v^- - \delta \end{aligned}$$

Receiver-side dereverberation by MDD
(Figure 12a)

$$\bar{R}_{\text{ddr}}^{\text{trc}} = (T_d^*)^{-1} \bar{R}_{\text{tar}} T_d = -(U_{R,R'}^{-,-})^{-1} U_{R,S'}^{-,+}$$

Source- and receiver-side dereverberation by
double extrapolated focusing (Figure 12b)

$$R_{\text{ddr}} = T_d^t R_{\text{tar}} T_d = v^{+t} \Psi_b^v R v^+$$

Primary retrieval (Figure 13)

$$\begin{aligned} R_{\text{prm}} &= T_d^t r T_d \quad (\text{for all depths}) \\ &= \left(R \sum_{k=0}^K \{\bar{\Theta}_a^v R^* \bar{\Theta}_b^v R\}^k \delta \right)_{t=t_2} \end{aligned}$$

Transmission-loss compensated primary retrieval (Figure 16)

$$\begin{aligned} R_{\text{prm}}^{\text{trc}} &= \{T_d^*\}^{-1} r T_d \quad (\text{for all depths}) \\ &= \left(R \sum_{k=0}^K \{\bar{\Theta}_a^v R^* \bar{\Theta}_b^{\epsilon,v} R\}^k \delta \right)_{t=t_2} \end{aligned}$$

Plane-wave primary retrieval

$$\begin{aligned} \tilde{R}_{\text{prm}} &= T_d^t r \tilde{T}_d \quad (\text{for all depths}) \\ &= \left(R \sum_{k=0}^K \{\tilde{\Theta}_a^v R^* \tilde{\Theta}_b^v R\}^k \tilde{\delta} \right)_{t=t_2 + \mathbf{p} \cdot \mathbf{x}_{H,R}} \end{aligned}$$

Plane-wave transmission-loss compensated primary retrieval (Figure 18)

$$\begin{aligned} \tilde{R}_{\text{prm}}^{\text{trc}} &= \{T_d^*\}^{-1} r \tilde{T}_d \quad (\text{for all depths}) \\ &= \left(R \sum_{k=0}^K \{\tilde{\Theta}_a^v R^* \tilde{\Theta}_b^{\epsilon,v} R\}^k \tilde{\delta} \right)_{t=t_2 + \mathbf{p} \cdot \mathbf{x}_{H,R}} \end{aligned}$$

MARCHENKO MULTIPLE ELIMINATION

All redatuming methods discussed in the section “Marchenko redatuming and imaging” have in common that internal multiples are eliminated between the surface and the virtual sources and/or receivers in the subsurface. The required input for these methods consists of the reflection response at the surface (after surface-related multiple elimination and deconvolution for the wavelet) and the direct arrivals of the focusing functions. The latter can be derived, for example, from a macro velocity model of the subsurface.

Meles et al. (2016) propose to extrapolate the virtual receivers (or, equivalently, the virtual sources) upward to the acquisition surface, using direct-wave Green’s functions. The result is a reflection response with sources and receivers at the surface, from which a part of the internal multiples are eliminated. Since the direct-wave Green’s functions are defined in the same velocity model as the direct arrivals of the focusing functions, the combined process of focusing and upward extrapolation is significantly less sensitive to errors in the velocity model than focusing as a stand-alone process.

Building on this idea, several Marchenko-based methods have been developed that extrapolate the virtual sources and receivers to the surface. However, instead of applying the extrapolation after Marchenko redatuming, in these methods the extrapolation operator is integrated in the Marchenko method. Since these methods yield reflection data at the surface with less internal multiples (van der Neut and Wapenaar, 2016), or even without any internal multiples (Zhang et al., 2019b), we refer to these methods as ‘Marchenko multiple elimination’ (opposed to ‘Marchenko redatuming’, which yields reflection data with less internal multiples at a datum plane in the subsurface).

Marchenko multiple elimination operates in the same domain as other internal multiple elimination methods in the literature (Weglein et al., 1997, 2003; Berkhout and Verschuur, 1997; Jakubowicz, 1998; ten Kroode, 2002; van Borselen, 2002; Verschuur and Berkhout, 2005; Ikelle, 2006). A comparison with these methods is beyond the scope of this paper. A specific characteristic of Marchenko multiple elimination is that it predicts and subtracts all orders of internal multiples with correct amplitudes. In the following we discuss Marchenko multiple elimination methods step-by-step.

Representations extrapolated to the surface

We use the direct arrival of the transmission response of the truncated medium, $T_d(\mathbf{x}_A, \mathbf{x}_S, t)$, as an operator to extrapolate wavefield quantities from \mathbb{S}_A

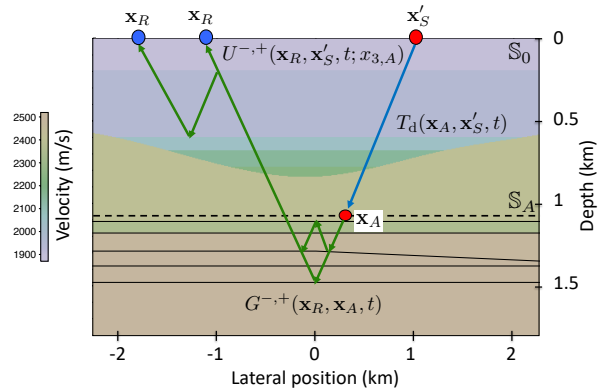


FIG. 9 Visualization of equation 59 (extrapolation of the source from \mathbf{x}_A at \mathbb{S}_A to \mathbf{x}'_S at the surface \mathbb{S}_0).

in the subsurface to the acquisition surface \mathbb{S}_0 . According to equation 17, the direct arrivals of the transmission response and of the focusing function are each other’s (band-limited) inverse. Here we reformulate equation 17 in terms of an integral along \mathbb{S}_A , as follows

$$\delta(\mathbf{x}_{H,R} - \mathbf{x}'_{H,S})\delta(t) = \int_{\mathbb{S}_A} d\mathbf{x}_A \int_{-\infty}^t f_{1,d}^+(\mathbf{x}_R, \mathbf{x}_A, t') T_d(\mathbf{x}_A, \mathbf{x}'_S, t - t') dt', \quad (57)$$

with \mathbf{x}_R and \mathbf{x}'_S at \mathbb{S}_0 . We use the operation $\int_{\mathbb{S}_A} d\mathbf{x}_A \int_{-\infty}^t \{\cdot\} T_d(\mathbf{x}_A, \mathbf{x}'_S, t - t') dt'$ to define the extrapolated focusing functions and Green’s functions as

$$v^\pm(\mathbf{x}_R, \mathbf{x}'_S, t; x_{3,A}) = \int_{\mathbb{S}_A} d\mathbf{x}_A \int_{-\infty}^t f_{1,d}^\pm(\mathbf{x}_R, \mathbf{x}_A, t') T_d(\mathbf{x}_A, \mathbf{x}'_S, t - t') dt' \quad (58)$$

and

$$U^{-,\pm}(\mathbf{x}_R, \mathbf{x}'_S, \pm t; x_{3,A}) = \int_{\mathbb{S}_A} d\mathbf{x}_A \int_{-\infty}^t G^{-,\pm}(\mathbf{x}_R, \mathbf{x}_A, \pm t') T_d(\mathbf{x}_A, \mathbf{x}'_S, t - t') dt', \quad (59)$$

respectively (van der Neut and Wapenaar, 2016). Equation 59 for $U^{-,+}(\mathbf{x}_R, \mathbf{x}'_S, t; x_{3,A})$ describes the extrapolation of the source of $G^{-,+}(\mathbf{x}_R, \mathbf{x}_A, t)$ from \mathbf{x}_A at \mathbb{S}_A to \mathbf{x}'_S at the surface \mathbb{S}_0 . The resulting response $U^{-,+}(\mathbf{x}_R, \mathbf{x}'_S, t; x_{3,A})$ can be interpreted as the reflection response between \mathbf{x}'_S and \mathbf{x}_R at the surface \mathbb{S}_0 , in which the wave field between the source at \mathbf{x}'_S and \mathbb{S}_A (at depth $x_{3,A}$) consists of the direct downgoing wave only. This is visualized in Figure 9.

Applying the same extrapolation operation to the left- and right-hand sides of equations 4 and 5, we

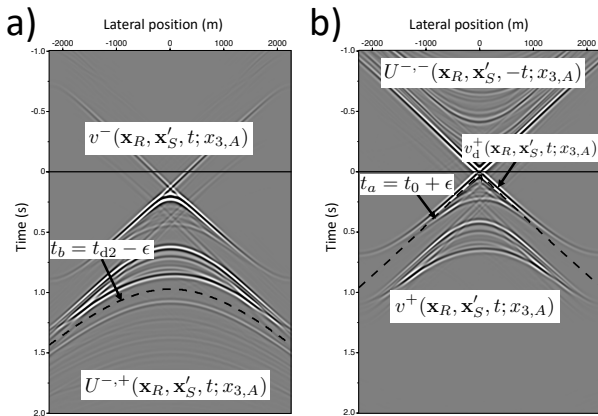


FIG. 10 (a) The left-hand side of equation 60 (fixed \mathbf{x}'_S , variable \mathbf{x}_R). (b) The left-hand side of equation 61.

obtain

$$U^{-,+}(\mathbf{x}_R, \mathbf{x}'_S, t; x_{3,A}) + v^{-}(\mathbf{x}_R, \mathbf{x}'_S, t; x_{3,A}) = (60) \int_{\mathbb{S}_0} d\mathbf{x}_S \int_0^{\infty} R(\mathbf{x}_R, \mathbf{x}_S, t') v^{+}(\mathbf{x}_S, \mathbf{x}'_S, t - t'; x_{3,A}) dt'$$

and

$$U^{-,-}(\mathbf{x}_R, \mathbf{x}'_S, -t; x_{3,A}) + v^{+}(\mathbf{x}_R, \mathbf{x}'_S, t; x_{3,A}) = (61) \int_{\mathbb{S}_0} d\mathbf{x}_S \int_{-\infty}^0 R(\mathbf{x}_R, \mathbf{x}_S, -t') v^{-}(\mathbf{x}_S, \mathbf{x}'_S, t - t'; x_{3,A}) dt'$$

The functions on the left-hand sides of equations 60 and 61, convolved with a wavelet, are shown in grey-level display in Figures 10a and 10b, respectively.

Retrieval of extrapolated focusing functions

To determine the window functions for suppressing the extrapolated Green's functions from equations 60 and 61, we need to know the first possible arrival of $U^{-,+}(\mathbf{x}_R, \mathbf{x}'_S, t; x_{3,A})$ and the last arrival of the time-reversed function $U^{-,-}(\mathbf{x}_R, \mathbf{x}'_S, -t; x_{3,A})$. The first possible arrival of $U^{-,+}(\mathbf{x}_R, \mathbf{x}'_S, t; x_{3,A})$ (which would occur when there would be a reflector just below \mathbb{S}_A) is obtained by substituting equation 6 into equation 59, hence

$$\{U^{-,+}(\mathbf{x}_R, \mathbf{x}'_S, t; x_{3,A})\}_{\text{first}} \propto (62) \int_{\mathbb{S}_A} d\mathbf{x}_A \int_0^t T_d(\mathbf{x}_R, \mathbf{x}_A, t') T_d(\mathbf{x}_A, \mathbf{x}'_S, t - t') dt'$$

Note that T_d is convolved with itself and integrated along \mathbb{S}_A . The main contribution comes from the stationary point on \mathbb{S}_A , which corresponds to the specular reflection point, see Figure 11a. Hence, this integral yields the direct arrival of the reflection response of the hypothetical reflector just below \mathbb{S}_A .

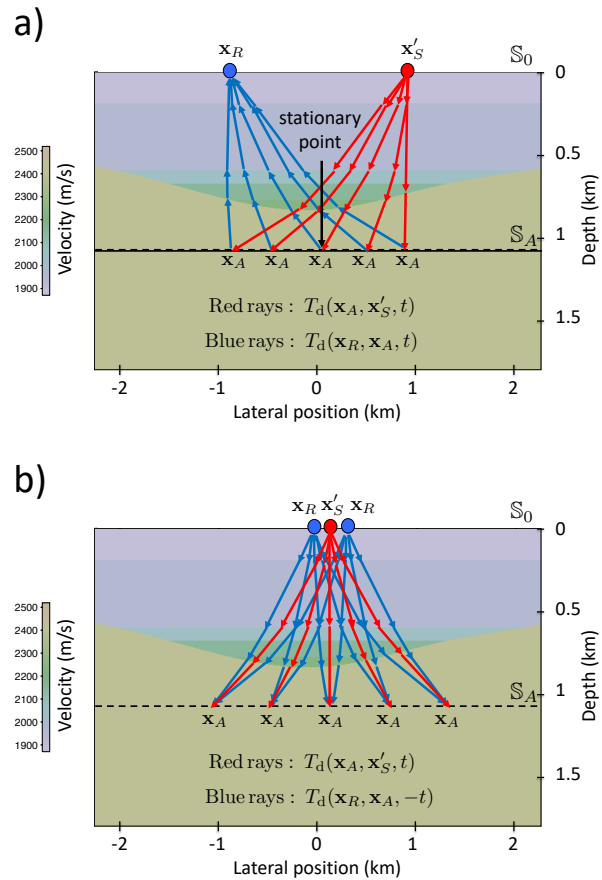


FIG. 11 (a) Visualization of equation 62. Convolution of the transmission responses yields a reflection response (the ray via the stationary point). (b) Visualization of equation 63. Correlation of the transmission responses yields a band-limited focus around \mathbf{x}'_S .

The arrival time of this event is the two-way traveltime $t_{d2}(\mathbf{x}_R, \mathbf{x}'_S; x_{3,A})$. Hence, $U^{-,+}(\mathbf{x}_R, \mathbf{x}'_S, t; x_{3,A})$ can be suppressed from equation 60 by a time window that removes everything beyond $t = t_b = t_{d2}(\mathbf{x}_R, \mathbf{x}'_S; x_{3,A}) - \epsilon$ (the dashed line in Figure 10a). The last arrival of $U^{-,-}(\mathbf{x}_R, \mathbf{x}'_S, -t; x_{3,A})$ is obtained by substituting equation 7 into equation 59, hence

$$\{U^{-,-}(\mathbf{x}_R, \mathbf{x}'_S, -t; x_{3,A})\}_{\text{last}} = (63) - \int_{\mathbb{S}_A} d\mathbf{x}_A \int_{-\infty}^0 T_d(\mathbf{x}_R, \mathbf{x}_A, -t') T_d(\mathbf{x}_A, \mathbf{x}'_S, t - t') dt'$$

Opposed to equation 62, here T_d is correlated with itself and integrated along \mathbb{S}_A , see Figure 11b. Hence, this integral yields a band-limited focus around $\mathbf{x}_R = \mathbf{x}'_S$ and $t = 0$. We denote the traveltime curve of this focus at positive time as $t_0(\mathbf{x}'_S, \mathbf{x}'_S)$. This is zero for zero-offset (i.e., $t_0(\mathbf{x}'_S, \mathbf{x}'_S) = 0$) and increases linearly with increasing offset between \mathbf{x}'_S and \mathbf{x}_R . Hence, $U^{-,-}(\mathbf{x}_R, \mathbf{x}'_S, -t; x_{3,A})$ can be suppressed from equation 61 by a time window that removes everything before $t = t_a = t_0(\mathbf{x}_R, \mathbf{x}'_S) + \epsilon$ (the dashed line in

Figure 10b). We define two time windows as

$$\Theta_a^v(\mathbf{x}_R, \mathbf{x}'_S, t; x_{3,A}) = \theta(t - t_a) = \theta(t - t_0 - \epsilon), \quad (64)$$

$$\Theta_b^v(\mathbf{x}_R, \mathbf{x}'_S, t; x_{3,A}) = \theta(t_b - t) = \theta(t_{d2} - \epsilon - t). \quad (65)$$

These windows suppress the extrapolated Green's functions and pass the extrapolated focusing functions v^+ and v^- (hence the superscript v in $\Theta_{a,b}^v$), except the extrapolated direct arrival $v_d^+(\mathbf{x}_R, \mathbf{x}'_S, t; x_{3,A})$, which coincides with the last arrival of $U^{-,-}(\mathbf{x}_R, \mathbf{x}'_S, -t; x_{3,A})$, see Figure 10b. This extrapolated direct arrival is, analogous to equation 58, defined as

$$v_d^+(\mathbf{x}_R, \mathbf{x}'_S, t; x_{3,A}) = \int_{\mathbb{S}_A} d\mathbf{x}_A \int_{-\infty}^t f_{1,d}^+(\mathbf{x}_R, \mathbf{x}_A, t') T_d(\mathbf{x}_A, \mathbf{x}'_S, t - t') dt', \quad (66)$$

or, using equation 57,

$$v_d^+(\mathbf{x}_R, \mathbf{x}'_S, t; x_{3,A}) = \delta(\mathbf{x}_{H,R} - \mathbf{x}'_{H,S}) \delta(t), \quad (67)$$

where the delta functions should be interpreted again in a band-limited sense.

Application of the windows $\Theta_{a,b}^v(\mathbf{x}_R, \mathbf{x}'_S, t; x_{3,A})$ to both sides of equations 60 and 61 gives, in the compact operator notation,

$$v^- = \Theta_b^v R v^+, \quad (68)$$

$$v^+ = \Theta_a^v R^* v^- + v_d^+, \quad (69)$$

with $v_d^+ = \delta$, see equation 67. These are the Marchenko equations for the extrapolated focusing functions. They can be solved, analogous to equation 16, by

$$v^+ = \sum_{k=0}^K \{\Theta_a^v R^* \Theta_b^v R\}^k \delta. \quad (70)$$

An important difference with equation 16 is that equation 70 does not contain the direct arrival of the focusing function, $f_{1,d}^+$. Instead it contains the delta function which, according to equation 67, depends only on the lateral source position $\mathbf{x}'_{H,S}$ but not on a model of the medium. This is a significant advantage of the Marchenko scheme of equation 70 over that of equation 16. Note that the window function Θ_b^v contains the two-way traveltime $t_{d2}(\mathbf{x}_R, \mathbf{x}'_S; x_{3,A})$ and hence implicitly depends on the medium. However, according to our experience, errors in the window functions have much less effect on the retrieved focusing functions than errors in the estimated direct arrival $f_{1,d}^+$ in equation 16.

Similar assumptions as discussed below equation 9 apply for the retrieval of the extrapolated focusing functions. Elison et al. (2020) discuss how to account for thin layering, assuming the medium between \mathbb{S}_0 and \mathbb{S}_A is horizontally layered.

The essential expressions for the retrieval of the extrapolated focusing functions, i.e., the Marchenko equations and the Marchenko scheme in the compact operator form, are summarized in Box 2. This box also shows the main expressions for the other methods discussed in the current section ‘‘Marchenko multiple elimination’’.

Retrieval of extrapolated Green's functions (source-side dereverberation)

The next step is the retrieval of the extrapolated Green's functions. We define the complementary time windows as

$$\Psi_{a,b}^v(\mathbf{x}_R, \mathbf{x}'_S, t; x_{3,A}) = 1 - \Theta_{a,b}^v(\mathbf{x}_R, \mathbf{x}'_S, t; x_{3,A}). \quad (71)$$

Application of these windows to both sides of equations 60 and 61 gives, in the compact operator notation,

$$U_{R,S'}^{-,+} = \Psi_b^v R v^+, \quad (72)$$

$$U_{R,S'}^{-,*} = \Psi_a^v R^* v^- - v_d^+, \quad (73)$$

where the subscripts on the left-hand sides refer to the position of the actual receiver and the extrapolated virtual source, both at \mathbb{S}_0 .

We interpret equation 72 as follows. The extrapolated focusing function v^+ is applied to the reflection response R at the surface \mathbb{S}_0 . The result is $U_{R,S'}^{-,+}$, which is the reflection response at the surface \mathbb{S}_0 , in which the wave field between the source at \mathbf{x}'_S and \mathbb{S}_A consists of the direct downgoing wave only (Figure 9). Since the multiples in the downgoing wave field are removed, we refer to the process described by equation 72 as dereverberation at the source side. Hence, where applicable, we call the extrapolated focusing function v^+ a dereverberation operator.

Before we discuss dereverberation at the receiver side, we spend some more words on equation 72. Substitution of equation 70 for v^+ yields

$$U_{R,S'}^{-,+} = \Psi_b^v [R - (-R\Theta_a^v R^* \Theta_b^v R) - (-R\Theta_a^v R^* \Theta_b^v R \Theta_a^v R^* \Theta_b^v R) \cdots]. \quad (74)$$

The first term between the square brackets is the reflection response. The subsequent terms predict internal multiples, which are subtracted from the reflection response. Note that the internal multiples are predicted via correlations and convolutions of the reflection response with itself. Jakubowicz (1998) introduced the prediction of first-order internal multiples as (in our notation) $-RR^*R$, where specific events have to be selected in the different versions of R in this expression. Hence, equation 74 or, more generally, equation 72 with v^+ defined in equation 70, can be seen as a generalization of the method proposed

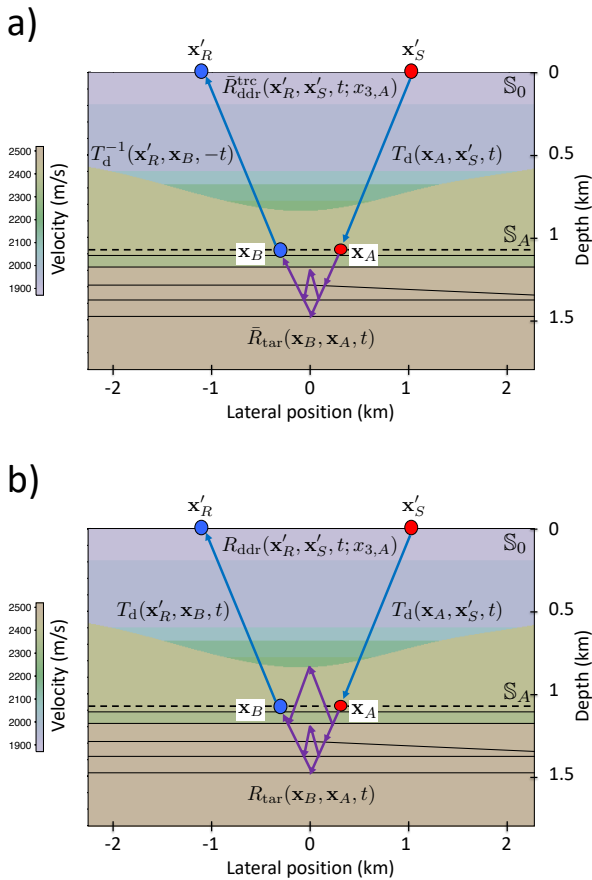


FIG. 12 (a) Visualization of equation 79. The purple rays represent the target reflection response at \mathbb{S}_A in the truncated medium (shown in more detail in Figure 4b). (b) Visualization of equation 85. The purple rays represent the target reflection response at \mathbb{S}_A in the actual medium (shown in more detail in Figure 4a).

by Jakubowicz (1998), for predicting and subtracting all orders of internal multiple reflections on the source side between \mathbb{S}_0 and \mathbb{S}_A . The window functions $\Theta_{a,b}^v$ and Ψ_b^v , defined in equations 64, 65 and 71, take care of the proper selection of the events that take part in the multiple prediction. In the following we discuss different methods to predict and subtract also the internal multiples on the receiver side.

Receiver-side dereverberation by MDD

Analogous to equation 23, which underlies redatuming by MDD, we formulate the following relation between the extrapolated Green's functions

$$U^{-,+}(\mathbf{x}_R, \mathbf{x}'_S, t) = - \int_{\mathbb{S}_0} d\mathbf{x}'_R \int_0^t U^{-,-}(\mathbf{x}_R, \mathbf{x}'_R, t') \times \bar{R}_{ddr}^{trc}(\mathbf{x}'_R, \mathbf{x}'_S, t - t'; x_{3,A}) dt'. \quad (75)$$

Whereas equation 23 is derived from wave theory, with $\bar{R}_{tar}(\mathbf{x}_B, \mathbf{x}_A, t)$ being the target reflection response of the truncated medium (Figure 4b), equation 75 is introduced purely on basis of analogy with equation 23. Hence, the physical meaning of $\bar{R}_{ddr}^{trc}(\mathbf{x}'_R, \mathbf{x}'_S, t; x_{3,A})$ still needs to be derived and the sub- and superscripts will be explained later. We start by rewriting equation 75 in the compact operator notation, as follows

$$U_{R,S'}^{-,+} = -U_{R,R'}^{-,-} \bar{R}_{ddr}^{trc}. \quad (76)$$

Upon substitution of equation 59 we obtain

$$G_{R,A}^{-,+} T_d = -G_{R,B}^{-,-} T_d^* \bar{R}_{ddr}^{trc}, \quad (77)$$

hence

$$\bar{R}_{ddr}^{trc} = -(T_d^*)^{-1} (G_{R,B}^{-,-})^{-1} G_{R,A}^{-,+} T_d. \quad (78)$$

On the right-hand side, we recognize $-(G_{R,B}^{-,-})^{-1} G_{R,A}^{-,+}$ as the redatuming-by-MDD algorithm of equation 25, which gives \bar{R}_{tar} , hence

$$\bar{R}_{ddr}^{trc} = (T_d^*)^{-1} \bar{R}_{tar} T_d. \quad (79)$$

Note that $(T_d^*)^{-1}$ is the inverse of the time-reversed direct arrival of the transmission response of the medium between \mathbb{S}_0 and \mathbb{S}_A (where the inverse is understood in the sense of integral equation 57, hence $(T_d^*)^{-1} = f_{1,d}^{+,*}$). Note that $(T_d^*)^{-1}$ has the same traveltimes as T_d , but different amplitudes. Whereas T_d includes transmission losses of the interfaces between \mathbb{S}_0 and \mathbb{S}_A , $(T_d^*)^{-1}$ compensates for such transmission losses. For the interpretation of equation 79 we refer to Figure 12a, which shows that $\bar{R}_{ddr}^{trc}(\mathbf{x}'_R, \mathbf{x}'_S, t; x_{3,A})$ can be seen as the reflection response between \mathbf{x}'_S and \mathbf{x}'_R at the surface \mathbb{S}_0 , in which the wave fields between \mathbb{S}_0 and \mathbb{S}_A consist of direct downgoing and upgoing waves only, and the response \bar{R}_{tar} at \mathbb{S}_A includes primaries and multiples of the target below \mathbb{S}_A (Figure 4b). Hence, \bar{R}_{ddr}^{trc} is the reflection response at \mathbb{S}_0 , double-dereverberated at the source and the receiver side (denoted by the subscript 'ddr'), and compensated for transmission losses in the medium between \mathbb{S}_0 and \mathbb{S}_A (denoted by superscript 'trc'). The transmission-loss compensation would be exact when T_d and $(T_d^*)^{-1}$ would see the same interfaces, which is the case in horizontally layered media (Elison et al., 2020); in laterally varying media the transmission-loss compensation is approximate.

Next we derive the algorithm for retrieving \bar{R}_{ddr}^{trc} from the reflection response R . From equation 76 we obtain

$$\bar{R}_{ddr}^{trc} = -(U_{R,R'}^{-,-})^{-1} U_{R,S'}^{-,+}, \quad (80)$$

with $U_{R,S'}^{-,+}$ and $U_{R,R'}^{-,-}$ retrieved from equations 72 and 73. Equation 80 accomplishes receiver-side dereverberation by MDD. The algorithm is similar to receiver redatuming by MDD (equation 25), but it is signifi-

cantly less sensitive to a model of the medium, see the discussion below equation 70. This is also explained by the fact that the sources and receivers of the input data $R(\mathbf{x}_R, \mathbf{x}_S, t)$ stay at the surface \mathbb{S}_0 in the output data $\bar{R}_{\text{ddr}}^{\text{trc}}(\mathbf{x}'_R, \mathbf{x}'_S, t; x_{3,A})$, instead of being re-datumed to \mathbb{S}_A as in $\bar{R}_{\text{tar}}(\mathbf{x}_B, \mathbf{x}_A, t)$. A numerical example is shown by van der Neut and Wapenaar (2016). Dukalski and de Vos (2020) solve equation 76 for $\bar{R}_{\text{ddr}}^{\text{trc}}$ with an easier-than-MDD inversion. In the next section we derive an alternative double dereverberation method, which also avoids the MDD process.

Source- and receiver-side dereverberation by double extrapolated focusing

Analogous to equation 26, which formulates receiver redatuming, we apply the dereverberation operator $v^+(\mathbf{x}_R, \mathbf{x}'_R, t; x_{3,A})$ to the receiver side of the extrapolated Green's function $U^{-,+}(\mathbf{x}_R, \mathbf{x}'_S, t; x_{3,A})$, according to

$$R_{\text{ddr}}(\mathbf{x}'_R, \mathbf{x}'_S, t; x_{3,A}) = \int_{\mathbb{S}_0} d\mathbf{x}_R \int_0^\infty v^+(\mathbf{x}_R, \mathbf{x}'_R, t - t'; x_{3,A}) \times U^{-,+}(\mathbf{x}_R, \mathbf{x}'_S, t'; x_{3,A}) dt' \quad (81)$$

(Dukalski and de Vos, 2020; Reinicke and Dukalski, 2020; Staring et al., 2021). To derive the physical meaning of $R_{\text{ddr}}(\mathbf{x}'_R, \mathbf{x}'_S, t; x_{3,A})$ on the left-hand side, we analyse the right-hand side step-by-step. In the compact operator notation, equation 81 becomes

$$R_{\text{ddr}} = v^{+,+} U_{R,S'}^{-,+}. \quad (82)$$

Upon substitution of equations 58 and 59 into equation 82, we obtain

$$R_{\text{ddr}} = T_d^t f_1^{+,+} G_{R,A}^{-,+} T_d, \quad (83)$$

or, upon substitution of equation 21,

$$R_{\text{ddr}} = T_d^t f_1^{+,+} (\Psi_b R f_1^+) T_d. \quad (84)$$

On the right-hand side, we recognize $f_1^{+,+} \Psi_b R f_1^+$ as the redatuming by double focusing algorithm of equation 28, which gives R_{tar} , hence

$$R_{\text{ddr}} = T_d^t R_{\text{tar}} T_d. \quad (85)$$

This equation describes the extrapolation of the source and receiver of $R_{\text{tar}}(\mathbf{x}_B, \mathbf{x}_A, t)$ from \mathbb{S}_A to the surface \mathbb{S}_0 , yielding $R_{\text{ddr}}(\mathbf{x}'_R, \mathbf{x}'_S, t; x_{3,A})$, see Figure 12b. $R_{\text{ddr}}(\mathbf{x}'_R, \mathbf{x}'_S, t; x_{3,A})$ is interpreted as the reflection response between \mathbf{x}'_S and \mathbf{x}'_R at the surface \mathbb{S}_0 , in which the wave fields between \mathbb{S}_0 and \mathbb{S}_A consist of the direct downgoing and upgoing waves only, and the response R_{tar} at \mathbb{S}_A includes primaries and multiples of the target below \mathbb{S}_A (and multiples between reflectors below and above \mathbb{S}_A , Figure 4a). Hence, R_{ddr} is

the reflection response at \mathbb{S}_0 , double-dereverberated at the source and the receiver side.

Next we derive the algorithm for retrieving R_{ddr} from the reflection response R . Substitution of equation 72 into equation 82 gives

$$R_{\text{ddr}} = v^{+,+} \Psi_b^v R v^+. \quad (86)$$

Equation 86 accomplishes double dereverberation by double extrapolated focusing. The algorithm is similar to redatuming by double focusing (equation 28), but it is significantly less sensitive to a model of the medium, because the sources and receivers stay at the surface.

Substituting equation 70 into equation 86, we obtain

$$R_{\text{ddr}} = \Psi_b^v R - (-\Psi_b^v R \Omega^v) - (-\Omega^{v,t} \Psi_b^v R) - (-\Omega^{v,t} \Psi_b^v R \Omega^v) + \dots, \quad (87)$$

with $\Omega^v = \Theta_a^v R^* \Theta_b^v R$. This is a similar expansion as equation 30 for redatuming by double focusing, but it lacks the direct arrival of the focusing function, $f_{1,d}^+$, which requires a macro subsurface model. In theory equation 87 converges. It allows an adaptive implementation of double dereverberation, to compensate for imperfections in the reflection response. Since the sources and receivers stay at the surface, the output R_{ddr} can be directly compared with the input data R , which is advantageous for quality control. Pereira et al. (2019) apply a modified version of this method to suppress first-order internal multiples from a 3D deep water OBN dataset. Reinicke and Dukalski (2020) and Staring et al. (2021) apply the method to shallow water numerical and field datasets, demonstrating the significance of including higher order terms to suppress internal multiples caused by a complex overburden.

Primary retrieval

The dereverberation methods discussed in the previous sections have in common that they remove internal multiples between the acquisition boundary \mathbb{S}_0 and a single, predefined boundary \mathbb{S}_A in the subsurface. Here we discuss a method for eliminating all internal multiples.

Our starting point is equation 72 which, after substitution of equation 70, becomes

$$U_{R,S'}^{-,+} = \Psi_b^v R \sum_{k=0}^K \{\Theta_a^v R^* \Theta_b^v R\}^k \delta. \quad (88)$$

This expression shows how to obtain the extrapolated Green's function $U^{-,+}(\mathbf{x}_R, \mathbf{x}'_S, t; x_{3,A})$ from the reflection data $R(\mathbf{x}_R, \mathbf{x}_S, t)$. According to equation 59, this

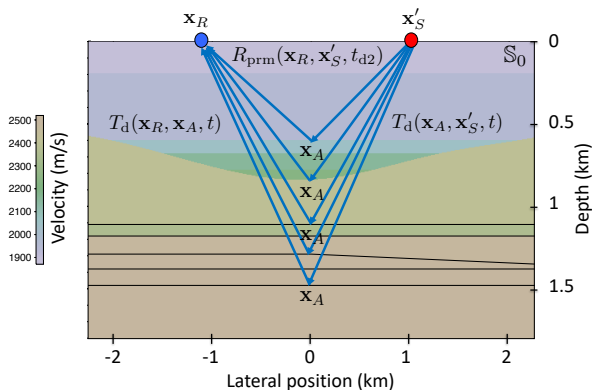


FIG. 13 Visualization of the primary response $R_{\text{prm}}(\mathbf{x}_R, \mathbf{x}'_S, t_{d2})$, obtained from equations 88, 89 and 90 for all $x_{3,A}$.

extrapolated Green's function is interpreted as the reflection response between \mathbf{x}'_S and \mathbf{x}_R at the surface \mathbb{S}_0 , in which the wave field between the source at \mathbf{x}'_S and \mathbb{S}_A (at depth $x_{3,A}$) consists of the direct down-going wave only, see Figure 9. In equation 62 and Figure 11a we showed that the first possible arrival of this response, denoted as $\{U^{-,+}(\mathbf{x}_R, \mathbf{x}'_S, t; x_{3,A})\}_{\text{first}}$, is the primary reflection response of a hypothetical reflector directly below \mathbb{S}_A , with two-way traveltime $t_{d2}(\mathbf{x}_R, \mathbf{x}'_S; x_{3,A})$. Assuming the hypothetical reflector has a local reflection coefficient $r(\mathbf{x}_A)$, we may replace equation 62 by

$$\{U^{-,+}(\mathbf{x}_R, \mathbf{x}'_S, t; x_{3,A})\}_{\text{first}} = \int_{\mathbb{S}_A} d\mathbf{x}_A \int_0^t T_d(\mathbf{x}_R, \mathbf{x}_A, t') r(\mathbf{x}_A) T_d(\mathbf{x}_A, \mathbf{x}'_S, t - t') dt'. \quad (89)$$

When the reflectivity is angle-dependent, $r(\mathbf{x}_A)$ should actually be replaced by a kernel $r(\mathbf{x}'_A, \mathbf{x}_A, t)$, and extra integrals along \mathbb{S}_A and time should be included in equation 89 (Berkhout, 1982; de Bruin et al., 1990). For convenience we continue with the simple form of equation 89.

We introduce $R_{\text{prm}}(\mathbf{x}_R, \mathbf{x}'_S, t)$ as the primary reflection response of the medium at the surface \mathbb{S}_0 . It can be obtained by evaluating equation 88 for all $x_{3,A}$ and, for each $x_{3,A}$, assigning the time slice $t = t_{d2}(\mathbf{x}_R, \mathbf{x}'_S; x_{3,A})$ to $R_{\text{prm}}(\mathbf{x}_R, \mathbf{x}'_S, t)$, according to

$$R_{\text{prm}}(\mathbf{x}_R, \mathbf{x}'_S, t_{d2}) = \{U^{-,+}(\mathbf{x}_R, \mathbf{x}'_S, t; x_{3,A})\}_{t=t_{d2}(\mathbf{x}_R, \mathbf{x}'_S; x_{3,A})} \quad (90)$$

(van der Neut and Wapenaar, 2016). Since the window Ψ_b^v in equation 88 passes the selected time slice, we may remove this window function from this equation when its output $U^{-,+}$ is used in equation 90. When $x_{3,A}$ corresponds to the depth of an interface then, according to equation 89, $R_{\text{prm}}(\mathbf{x}_R, \mathbf{x}'_S, t_{d2})$ for the corresponding two-way time t_{d2} represents the pri-

mary reflection response of that interface. When there is no interface at $x_{3,A}$, then $R_{\text{prm}}(\mathbf{x}_R, \mathbf{x}'_S, t_{d2})$ will be zero at the corresponding two-way time t_{d2} . Figure 13 visualizes $R_{\text{prm}}(\mathbf{x}_R, \mathbf{x}'_S, t_{d2})$ for all $x_{3,A}$.

Note that this method still requires an estimate of the velocity model to derive $t_{d2}(\mathbf{x}_R, \mathbf{x}'_S; x_{3,A})$ (which appears in the window function Θ_b^v in equation 88 as well as in equation 90). Furthermore, the time slices for varying $x_{3,A}$ will in general not cover the space-time domain $(\mathbf{x}_R, \mathbf{x}'_S, t)$ in a regular way. Both issues can be overcome by replacing the depth variable $x_{3,A}$ by the two-way traveltime t_2 along the vertical coordinate between $x_{3,0}$ and $x_{3,A}$ (hence, independent of \mathbf{x}_R and \mathbf{x}'_S), and by replacing the time window functions $\Theta_{a,b}^v(\mathbf{x}_R, \mathbf{x}'_S, t; x_{3,A})$ by

$$\bar{\Theta}_a^v(t; t_2) = \theta(t - \epsilon), \quad (91)$$

$$\bar{\Theta}_b^v(t; t_2) = \theta(t_2 - \epsilon - t) \quad (92)$$

(Zhang et al., 2019a). Making these replacements in equations 88 and 90, we obtain

$$R_{\text{prm}}(\mathbf{x}_R, \mathbf{x}'_S, t_2) = \{U^{-,+}(\mathbf{x}_R, \mathbf{x}'_S, t; t_2)\}_{t=t_2} \quad (93) \\ = \left(R \sum_{k=0}^K \{\bar{\Theta}_a^v R^* \bar{\Theta}_b^v R\}^k \delta \right)_{t=t_2}.$$

This equation shows how the primary reflection response $R_{\text{prm}}(\mathbf{x}_R, \mathbf{x}'_S, t_2)$ (called R_t by Zhang et al. (2019a)) is retrieved from the reflection data at the surface without needing any velocity information. Note that the space-independent window function $\bar{\Theta}_b^v$ cuts through offset-dependent events in the data. This aspect of the method is analysed in detail by Thorbecke et al. (2021). For a field data example we refer to Zhang and Slob (2020b).

Transmission-loss compensated primary retrieval

In the section ‘‘Receiver-side dereverberation by MDD’’, we showed that the response $\bar{R}_{\text{ddr}}^{\text{trc}}$, which is obtained by multidimensional deconvolution, is compensated for the transmission losses between \mathbb{S}_0 and \mathbb{S}_A (Figure 12a). Slob et al. (2014) showed for the 1D situation that a transmission-loss compensated local reflection coefficient can be obtained directly from the upgoing focusing function f_1^- , hence, without the need for deconvolution. Using the extrapolation method, it thus follows that a transmission-loss compensated primary reflection response at the surface of a local reflection event in the subsurface can be obtained directly from the extrapolated upgoing focusing function v^- . This idea was used by Zhang et al. (2019b), who developed a 3D method for retrieving the transmission-loss compensated primary response at the surface for all reflectors in the subsurface, without the need for MDD. Here we discuss this approach in detail.

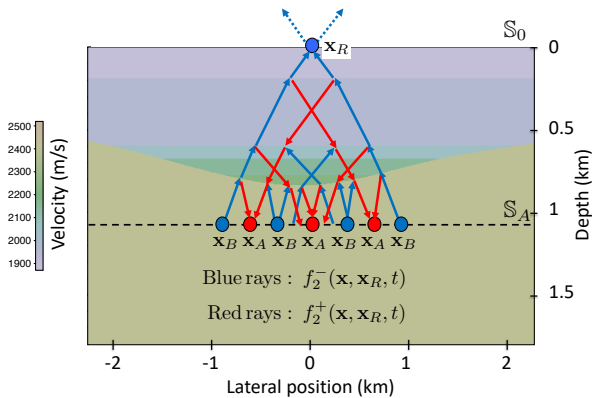


FIG. 14 Focusing functions f_2^- and f_2^+ in the truncated medium.

Before we analyze the extrapolated upgoing focusing function v^- , we discuss focusing functions $f_2^+(\mathbf{x}, \mathbf{x}_R, t)$ and $f_2^-(\mathbf{x}, \mathbf{x}_R, t)$, with \mathbf{x}_R at \mathbb{S}_0 , as counterparts of $f_1^+(\mathbf{x}, \mathbf{x}_A, t)$ and $f_1^-(\mathbf{x}, \mathbf{x}_A, t)$, with \mathbf{x}_A at \mathbb{S}_A . These focusing functions are defined in the same truncated medium, see Figure 14. The upgoing focusing function $f_2^-(\mathbf{x}_B, \mathbf{x}_R, t)$, with \mathbf{x}_B at \mathbb{S}_A , is defined such that $f_2^-(\mathbf{x}, \mathbf{x}_R, t)$ focuses at $\mathbf{x} = \mathbf{x}_R$ and $t = 0$ and continues as a diverging upgoing field into the homogeneous half-space above \mathbb{S}_0 . The formal focusing conditions are

$$f_2^+(\mathbf{x}'_R, \mathbf{x}_R, t) = 0, \quad (94)$$

$$f_2^-(\mathbf{x}'_R, \mathbf{x}_R, t) = \delta(\mathbf{x}'_{H,R} - \mathbf{x}_{H,R})\delta(t), \quad (95)$$

for \mathbf{x}'_R at \mathbb{S}_0 . The downgoing focusing function $f_2^+(\mathbf{x}_A, \mathbf{x}_R, t)$ is the response of the truncated medium to $f_2^-(\mathbf{x}_B, \mathbf{x}_R, t)$, observed at \mathbf{x}_A at \mathbb{S}_A . This is formulated as

$$f_2^+(\mathbf{x}_A, \mathbf{x}_R, t) = \int_{\mathbb{S}_A} d\mathbf{x}_B \int_0^\infty R^\cap(\mathbf{x}_A, \mathbf{x}_B, t') f_2^-(\mathbf{x}_B, \mathbf{x}_R, t - t') dt', \quad (96)$$

where $R^\cap(\mathbf{x}_A, \mathbf{x}_B, t)$ is the reflection response of the truncated medium ‘from below’. The following relations hold between f_1^\pm and f_2^\pm (Wapenaar et al., 2014)

$$f_1^+(\mathbf{x}_R, \mathbf{x}_A, t) = f_2^-(\mathbf{x}_A, \mathbf{x}_R, t), \quad (97)$$

$$f_1^-(\mathbf{x}_R, \mathbf{x}_A, t) = -f_2^+(\mathbf{x}_A, \mathbf{x}_R, -t), \quad (98)$$

see also the Appendix.

We now analyze the extrapolated upgoing focusing function $v^-(\mathbf{x}_R, \mathbf{x}'_S, t; x_{3,A})$, as defined by equation 58. Upon substitution of equation 98 we obtain

$$v^-(\mathbf{x}_R, \mathbf{x}'_S, t; x_{3,A}) = - \int_{\mathbb{S}_A} d\mathbf{x}_A \int_{-\infty}^t f_2^+(\mathbf{x}_A, \mathbf{x}_R, -t') T_d(\mathbf{x}_A, \mathbf{x}'_S, t - t') dt'. \quad (99)$$

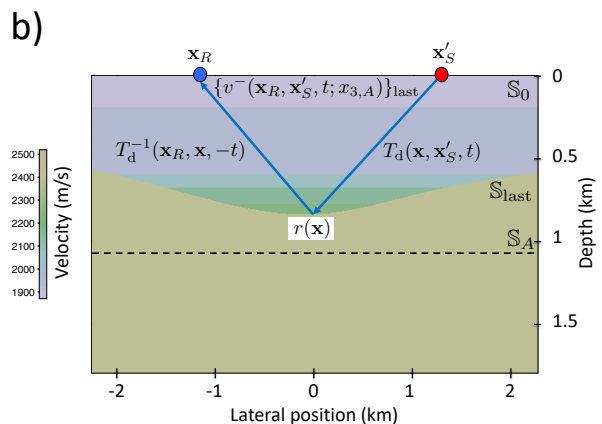
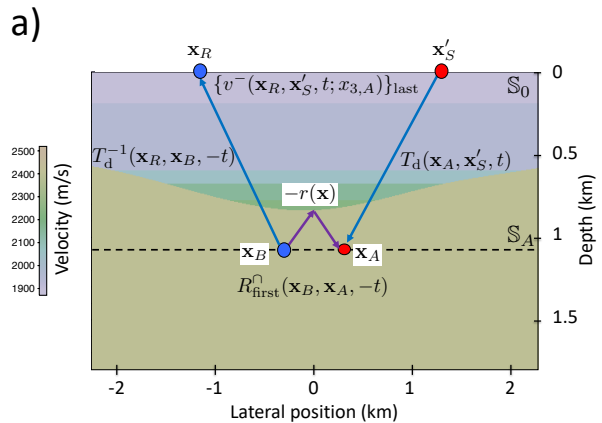


FIG. 15 (a) Visualization of equation 104. The purple rays represent the time-reversed reflection response at \mathbb{S}_A of the last reflector of the truncated medium above \mathbb{S}_A . (b) Visualization of equation 109 (the transmission-loss compensated primary response of the last interface above \mathbb{S}_A).

In the compact operator notation, this equation reads

$$v^- = -f_2^{+\star} T_d. \quad (100)$$

For f_2^+ we use equation 96 in which we substitute equation 97. This gives

$$f_2^+ = R^\cap f_1^{+\star}. \quad (101)$$

Substituting this into equation 100, using $R^{\cap t} = R^\cap$, yields

$$v^- = -f_1^{+\star} R^{\cap\star} T_d. \quad (102)$$

The last event of v^- is obtained by selecting the first events of R^\cap and f_1^+ , hence

$$v_{\text{last}}^- = -f_{1,d}^{+\star} R_{\text{first}}^{\cap\star} T_d, \quad (103)$$

or, using equation 17,

$$v_{\text{last}}^- = -(T_d^\star)^{-1} R_{\text{first}}^{\cap\star} T_d. \quad (104)$$

Here $(T_d^\star)^{-1}$ is the transmission-loss compensated di-

rect wave, see the discussion below equation 79. Equation 104 is visualized in Figure 15a. This figure shows that $\{v^-(\mathbf{x}_R, \mathbf{x}'_S, t; x_{3,A})\}_{\text{last}}$ is interpreted as a reflection response between \mathbf{x}'_S and \mathbf{x}_R at the surface \mathbb{S}_0 , in which the wave fields between \mathbb{S}_0 and \mathbb{S}_A consist of direct downgoing and transmission-loss compensated upgoing waves only, and the only reflection comes from the lower side of the last interface above \mathbb{S}_A . Next we express R_{first}^\cap as

$$R_{\text{first}}^\cap(\mathbf{x}_B, \mathbf{x}_A, t) = - \int_{\mathbb{S}_{\text{last}}} d\mathbf{x} \int_0^t w(\mathbf{x}_B, \mathbf{x}, t') r(\mathbf{x}) w(\mathbf{x}, \mathbf{x}_A, t - t') dt', \quad (105)$$

where \mathbb{S}_{last} represents the last interface of the truncated medium, $w(\mathbf{x}, \mathbf{x}_A, t)$ is an extrapolation operator for the homogeneous layer between \mathbb{S}_A and \mathbb{S}_{last} , and $r(\mathbf{x})$ with \mathbf{x} on \mathbb{S}_{last} is the local reflection coefficient of the last interface. The minus sign accounts for the fact that, in the acoustic approximation, the reflection coefficient at the lower side of an interface is the opposite of that at the upper side of the same interface. In the compact operator notation, equation 105 becomes

$$R_{\text{first}}^\cap = -w^t r_{\text{last}} w. \quad (106)$$

Substituting this into equation 104, using the fact that in the homogeneous layer we have $w^t = (w^*)^{-1}$, we obtain

$$v_{\text{last}}^- = (w T_d^*)^{-1} r_{\text{last}} (w^* T_d). \quad (107)$$

Here $w^* T_d$ is the direct arrival of the transmission response between \mathbb{S}_0 and \mathbb{S}_A , back-extrapolated from \mathbb{S}_A to \mathbb{S}_{last} , which we denote by $T_{d,\text{last}}$. Hence,

$$v_{\text{last}}^- = (T_{d,\text{last}}^*)^{-1} r_{\text{last}} T_{d,\text{last}}, \quad (108)$$

or

$$\{v^-(\mathbf{x}_R, \mathbf{x}'_S, t; x_{3,A})\}_{\text{last}} = \int_{\mathbb{S}_{\text{last}}} d\mathbf{x} \int_0^t T_d^{-1}(\mathbf{x}_R, \mathbf{x}, -t') r(\mathbf{x}) T_d(\mathbf{x}, \mathbf{x}'_S, t - t') dt'. \quad (109)$$

This equation is visualized in Figure 15b. It shows that $\{v^-(\mathbf{x}_R, \mathbf{x}'_S, t; x_{3,A})\}_{\text{last}}$ is the transmission-loss compensated primary reflection response of the last interface above \mathbb{S}_A (see also the discussion below equation 79).

Next we discuss a Marchenko scheme to retrieve $\{v^-(\mathbf{x}_R, \mathbf{x}'_S, t; x_{3,A})\}_{\text{last}}$ from the reflection response $R(\mathbf{x}_R, \mathbf{x}_S, t)$ at the surface. Equations 60 and 61 form again the basis for this. We need to define window functions that suppress the extrapolated Green's functions $U^{-,+}$ and $U^{-,-}$ from these equations, but preserve v_{last}^- , even when \mathbb{S}_A lies close to the reflector represented by v_{last}^- . If we would choose a hypothetical reflector just below \mathbb{S}_A , like we did in equa-

tion 62, this reflector would by definition lie outside the truncated medium and, hence, not contribute to $v^-(\mathbf{x}_R, \mathbf{x}'_S, t; x_{3,A})$. Instead we choose a hypothetical reflector just above \mathbb{S}_A (i.e., inside the truncated medium) and define the corresponding event as $\{v^-(\mathbf{x}_R, \mathbf{x}'_S, t; x_{3,A})\}_{\text{last}}$, with subscript 'last' standing for 'last possible'. Note that in this way we are approaching the hypothetical reflector from below, similar as we approached the actual last reflector from below in equation 104 and Figure 15a. Analogous to equation 109 we write

$$\{v^-(\mathbf{x}_R, \mathbf{x}'_S, t; x_{3,A})\}_{\text{last}} = \int_{\mathbb{S}_A} d\mathbf{x}_A \int_0^t T_d^{-1}(\mathbf{x}_R, \mathbf{x}_A, -t') r(\mathbf{x}_A) T_d(\mathbf{x}_A, \mathbf{x}'_S, t - t') dt', \quad (110)$$

where $r(\mathbf{x}_A)$ is the reflection coefficient of the hypothetical reflector. The arrival time of this event is again the two-way traveltime $t_{d2}(\mathbf{x}_R, \mathbf{x}'_S; x_{3,A})$. Hence, if we apply a time window to equation 60 that removes everything beyond $t = t_b = t_{d2}(\mathbf{x}_R, \mathbf{x}'_S; x_{3,A}) + \epsilon$, then v_{last}^- is preserved (and due to the finite bandwidth it is still preserved when \mathbb{S}_A lies less than half a wavelength above the hypothetical reflector (Zhang et al., 2019b)). We define this time window as

$$\Theta_b^{\epsilon,v}(\mathbf{x}_R, \mathbf{x}'_S, t; x_{3,A}) = \theta(t_b - t) = \theta(t_{d2} + \epsilon - t) \quad (111)$$

Since we replaced $t_{d2} - \epsilon$ from our previous window function (equation 65) by $t_{d2} + \epsilon$, the question arises whether this window still suppresses $U^{-,+}(\mathbf{x}_R, \mathbf{x}'_S, t; x_{3,A})$. To address this question, consider Figure 9 and keep in mind that \mathbf{x}_A lies just below the hypothetical reflector. Since the virtual source at \mathbf{x}_A radiates downward, the hypothetical reflector does not contribute to $U^{-,+}(\mathbf{x}_R, \mathbf{x}'_S, t; x_{3,A})$. Hence, the first event in $U^{-,+}$ arrives later than $t_{d2}(\mathbf{x}_R, \mathbf{x}'_S; x_{3,A}) + \epsilon$ (still assuming layers are not thin compared to the wavelength), so the proposed time window indeed suppresses $U^{-,+}(\mathbf{x}_R, \mathbf{x}'_S, t; x_{3,A})$ from equation 60. To suppress $U^{-,-}(\mathbf{x}_R, \mathbf{x}'_S, -t; x_{3,A})$ from equation 61 we need again the time window $\Theta_a^v(\mathbf{x}_R, \mathbf{x}'_S, t; x_{3,A})$ defined in equation 64, which removes everything before $t = t_a = t_0(\mathbf{x}_R, \mathbf{x}'_S) + \epsilon$. Applying the windows $\Theta_b^{\epsilon,v}$ and Θ_a^v to equations 60 and 61 we obtain, analogous to equations 68 and 70,

$$v^-(\mathbf{x}_R, \mathbf{x}'_S, t; x_{3,A}) = \Theta_b^{\epsilon,v} R \sum_{k=0}^K \{\Theta_a^v R^* \Theta_b^{\epsilon,v} R\}^k \delta. \quad (112)$$

The transmission-loss compensated primary reflection response $R_{\text{prm}}^{\text{trc}}(\mathbf{x}_R, \mathbf{x}'_S, t)$ can be obtained by evaluating equation 112 for all $x_{3,A}$ and, for each $x_{3,A}$, assigning the time slice $t = t_{d2}(\mathbf{x}_R, \mathbf{x}'_S; x_{3,A})$ to $R_{\text{prm}}^{\text{trc}}(\mathbf{x}_R, \mathbf{x}'_S, t)$, according to

$$R_{\text{prm}}^{\text{trc}}(\mathbf{x}_R, \mathbf{x}'_S, t_{d2}) = \{v^-(\mathbf{x}_R, \mathbf{x}'_S, t; x_{3,A})\}_{t=t_{d2}(\mathbf{x}_R, \mathbf{x}'_S; x_{3,A})}. \quad (113)$$

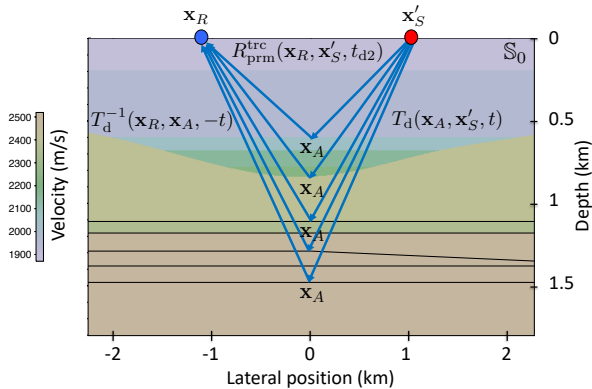


FIG. 16 Visualization of the transmission-loss compensated primary response $R_{\text{pr}m}^{\text{tr}c}(\mathbf{x}_R, \mathbf{x}'_S, t_{d2})$, obtained from equations 110, 112 and 113 for all $x_{3,A}$.

Since the leftmost window $\Theta_b^{\epsilon,v}$ in equation 112 passes the selected time slice, we may remove this window function from this equation when its output v^- is used in equation 113. Figure 16 visualizes $R_{\text{pr}m}^{\text{tr}c}(\mathbf{x}_R, \mathbf{x}'_S, t_{d2})$ for all $x_{3,A}$.

Next, using similar arguments as in the previous section, we replace the depth variable $x_{3,A}$ by the two-way traveltimes t_2 along the vertical coordinate between $x_{3,0}$ and $x_{3,A}$ (independent of \mathbf{x}_R and \mathbf{x}'_S), and the time window functions Θ_a^v and $\Theta_b^{\epsilon,v}$ by $\bar{\Theta}_a^v(t; t_2)$ defined in equation 91 and

$$\bar{\Theta}_b^{\epsilon,v}(t; t_2) = \theta(t_2 + \epsilon - t) \quad (114)$$

(Zhang et al., 2019b). Making these replacements in equations 112 and 113, we obtain

$$\begin{aligned} R_{\text{pr}m}^{\text{tr}c}(\mathbf{x}_R, \mathbf{x}'_S, t_2) &= \{v^-(\mathbf{x}_R, \mathbf{x}'_S, t; t_2)\}_{t=t_2} \quad (115) \\ &= \left(R \sum_{k=0}^K \{\bar{\Theta}_a^v R^* \bar{\Theta}_b^{\epsilon,v} R\}^k \delta \right)_{t=t_2}. \end{aligned}$$

This equation shows how the transmission-loss compensated primary reflection response $R_{\text{pr}m}^{\text{tr}c}(\mathbf{x}_R, \mathbf{x}'_S, t_2)$ (called R_r by Zhang et al. (2019b)) is retrieved from the reflection data at the surface without needing any velocity information. For numerical examples we refer to Zhang et al. (2019b) and for an efficient implementation to Zhang and Slob (2020a).

Plane-wave primary retrieval

In this section we integrate the plane-wave approach, introduced in the section ‘‘Plane-wave redatuming’’, with the transmission-loss compensated primary retrieval approach, introduced in the previous section. In this way we combine the numerical efficiency gain achieved by the plane-wave approach, with

the model-independency of the primary retrieval approach (Meles et al., 2020).

We define the extrapolated plane-wave focusing functions and Green’s functions, analogous to equations 41 and 43, as

$$\begin{aligned} \tilde{v}^{\pm}(\mathbf{x}_R, \mathbf{p}, t; x_{3,A}) &= \quad (116) \\ &= \int_{\mathbb{S}_0} v^{\pm}(\mathbf{x}_R, \mathbf{x}'_S, t - \mathbf{p} \cdot \mathbf{x}'_{H,S}; x_{3,A}) d\mathbf{x}'_S \end{aligned}$$

and

$$\begin{aligned} \tilde{U}^{-,\pm}(\mathbf{x}_R, \mathbf{p}, t; x_{3,A}) &= \quad (117) \\ &= \int_{\mathbb{S}_0} U^{-,\pm}(\mathbf{x}_R, \mathbf{x}'_S, t - \mathbf{p} \cdot \mathbf{x}'_{H,S}; x_{3,A}) d\mathbf{x}'_S. \end{aligned}$$

Note that the integration takes place along the extrapolated source positions \mathbf{x}'_S at the surface \mathbb{S}_0 , unlike in equations 41 and 43, where we integrate along the focal points \mathbf{x}_A at \mathbb{S}_A . Hence, the rayparameter vector $\mathbf{p} = (p_1, p_2)$ refers to a plane wave at the surface rather than at the focal depth. For an interpretation of $\tilde{U}^{-,+}(\mathbf{x}_R, \mathbf{p}, t; x_{3,A})$, substitute equation 59 into equation 117. This gives

$$\begin{aligned} \tilde{U}^{-,+}(\mathbf{x}_R, \mathbf{p}, t; x_{3,A}) &= \quad (118) \\ &= \int_{\mathbb{S}_A} d\mathbf{x}_A \int_0^t G^{-,+}(\mathbf{x}_R, \mathbf{x}_A, t') \tilde{T}_d(\mathbf{x}_A, \mathbf{p}, t - t') dt', \end{aligned}$$

with

$$\tilde{T}_d(\mathbf{x}_A, \mathbf{p}, t) = \int_{\mathbb{S}_0} T_d(\mathbf{x}_A, \mathbf{x}'_S, t - \mathbf{p} \cdot \mathbf{x}'_{H,S}) d\mathbf{x}'_S. \quad (119)$$

Hence, $\tilde{U}^{-,+}(\mathbf{x}_R, \mathbf{p}, t; x_{3,A})$ can be interpreted as the reflection response to a downgoing plane wave with rayparameter \mathbf{p} at the surface \mathbb{S}_0 , observed by a receiver at \mathbf{x}_R , in which the downgoing wave between the \mathbb{S}_0 and \mathbb{S}_A consists of the direct downgoing wave only. This is visualized in Figure 17a.

Applying equations 116 and 117 to the left- and right-hand sides of equations 60 and 61, we obtain

$$\begin{aligned} \tilde{U}^{-,+}(\mathbf{x}_R, \mathbf{p}, t; x_{3,A}) + \tilde{v}^-(\mathbf{x}_R, \mathbf{p}, t; x_{3,A}) &= \quad (120) \\ &= \int_{\mathbb{S}_0} d\mathbf{x}_S \int_0^{\infty} R(\mathbf{x}_R, \mathbf{x}_S, t') \tilde{v}^+(\mathbf{x}_S, \mathbf{p}, t - t'; x_{3,A}) dt' \end{aligned}$$

and

$$\begin{aligned} \tilde{U}^{-,-}(\mathbf{x}_R, -\mathbf{p}, -t; x_{3,A}) + \tilde{v}^+(\mathbf{x}_R, \mathbf{p}, t; x_{3,A}) &= \quad (121) \\ &= \int_{\mathbb{S}_0} d\mathbf{x}_S \int_{-\infty}^0 R(\mathbf{x}_R, \mathbf{x}_S, -t') \tilde{v}^-(\mathbf{x}_S, \mathbf{p}, t - t'; x_{3,A}) dt'. \end{aligned}$$

The functions on the left-hand sides of equations 120 and 121, convolved with a wavelet, are shown in grey-level display in Figures 17b and 17c, respectively.

We need time windows that separate the extrapolated plane-wave Green’s functions from the extrapo-

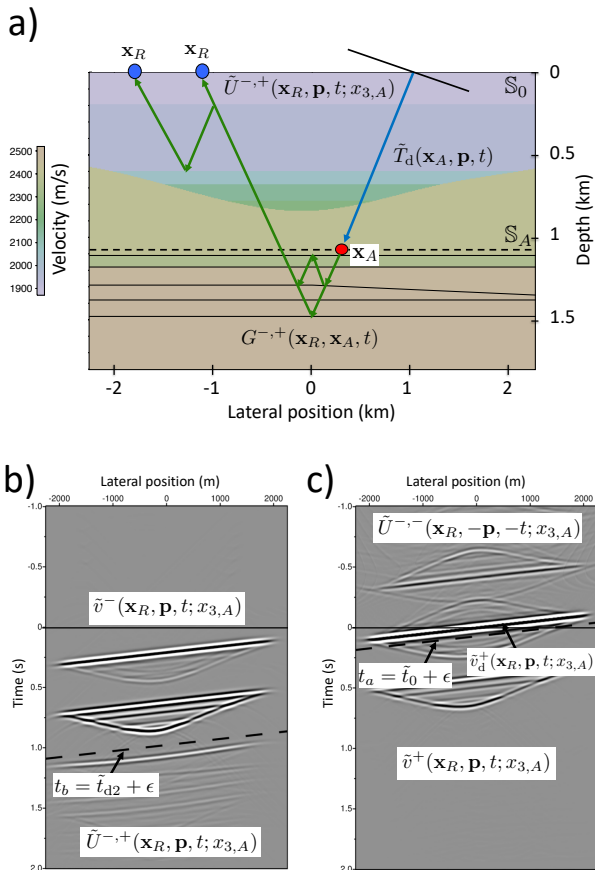


FIG. 17 (a) Visualization of the extrapolated plane-wave Green's function $\tilde{U}^{-,+}(\mathbf{x}_R, \mathbf{p}, t; x_{3,A})$ (here shown for a negative value of p_1 and $p_2 = 0$). (b) The left-hand side of equation 120 (fixed \mathbf{p} , variable \mathbf{x}_R). (c) The left-hand side of equation 121.

lated plane-wave focusing functions in equations 120 and 121. Similar as for the primary retrieval methods for extrapolated point sources, we can follow two approaches. If we would design a window $\tilde{\Theta}_b^v$ that suppresses $\tilde{U}^{-,+}(\mathbf{x}_R, \mathbf{p}, t; x_{3,A})$ from equation 120, including its first possible arrival from a hypothetical reflector just below \mathbb{S}_A , then, following an approach similar to that in the section “Primary retrieval”, we would obtain a method for plane-wave primary retrieval, without compensation for transmission losses. On the other hand, if we design a window $\tilde{\Theta}_b^{\epsilon,v}$ that preserves $\tilde{v}^{-}(\mathbf{x}_R, \mathbf{p}, t; x_{3,A})$ in equation 120, including its last possible arrival from a hypothetical reflector just above \mathbb{S}_A , then an approach similar to that in the section “Transmission-loss compensated primary retrieval” will lead to a method for plane-wave transmission-loss compensated primary retrieval. Both approaches are included in Box 2, but here we only discuss the second approach in more detail. Substituting equation 110 into equa-

tion 116, we obtain

$$\{\tilde{v}^{-}(\mathbf{x}_R, \mathbf{p}, t; x_{3,A})\}_{\text{last}'} = \int_{\mathbb{S}_A} d\mathbf{x}_A \int_0^t T_d^{-1}(\mathbf{x}_R, \mathbf{x}_A, -t') r(\mathbf{x}_A) \tilde{T}_d(\mathbf{x}_A, \mathbf{p}, t - t') dt'. \quad (122)$$

This is interpreted as the transmission-loss compensated primary reflection response to a dipping plane wave emitted from \mathbb{S}_0 with rayparameter \mathbf{p} and arriving at \mathbf{x}_R via a hypothetical reflector just above \mathbb{S}_A . We denote the arrival time of this event as $\tilde{t}_{d2}(\mathbf{x}_R, \mathbf{p}; x_{3,A})$. Hence, if we apply a time window to equation 120 that removes everything beyond $t = t_b = \tilde{t}_{d2}(\mathbf{x}_R, \mathbf{p}; x_{3,A}) + \epsilon$ (the dashed line in Figure 17b), then $\{\tilde{v}^{-}(\mathbf{x}_R, \mathbf{p}, t; x_{3,A})\}_{\text{last}'}$ is preserved (note that in this specific example the actual last reflector above \mathbb{S}_A is not close to \mathbb{S}_A in Figure 17a, and hence the last event of $\tilde{v}^{-}(\mathbf{x}_R, \mathbf{p}, t; x_{3,A})$ in Figure 17b is not close to the dashed line).

The window for equation 121 will be designed such that it suppresses $\tilde{U}^{-,-}(\mathbf{x}_R, -\mathbf{p}, -t; x_{3,A})$. Substituting equation 63 into equation 117 gives

$$\{\tilde{U}^{-,-}(\mathbf{x}_R, -\mathbf{p}, -t; x_{3,A})\}_{\text{last}} = - \int_{\mathbb{S}_A} d\mathbf{x}_A \int_{-\infty}^0 T_d(\mathbf{x}_R, \mathbf{x}_A, -t') \tilde{T}_d(\mathbf{x}_A, \mathbf{p}, t - t') dt'. \quad (123)$$

This is interpreted as the back-extrapolation of the plane-wave response $\tilde{T}_d(\mathbf{x}_A, \mathbf{p}, t)$ from \mathbb{S}_A to \mathbb{S}_0 , which gives the original plane wave at \mathbb{S}_0 with rayparameter \mathbf{p} . The arrival time of this event is $\tilde{t}_0(\mathbf{x}_R, \mathbf{p}) = \mathbf{p} \cdot \mathbf{x}_{H,R}$. Hence, $\tilde{U}^{-,-}(\mathbf{x}_R, -\mathbf{p}, -t; x_{3,A})$ can be suppressed from equation 121 by a time window that removes everything before $t = t_a = \mathbf{p} \cdot \mathbf{x}_{H,R} + \epsilon$ (the dashed line in Figure 17c, indicated by $t_0 + \epsilon$). We define the two time windows as

$$\tilde{\Theta}_a^v(\mathbf{x}_R, \mathbf{p}, t; x_{3,A}) = \theta(t - \mathbf{p} \cdot \mathbf{x}_{H,R} - \epsilon), \quad (124)$$

$$\tilde{\Theta}_b^{\epsilon,v}(\mathbf{x}_R, \mathbf{p}, t; x_{3,A}) = \theta(\tilde{t}_{d2} + \epsilon - t). \quad (125)$$

These windows pass the extrapolated plane-wave focusing functions \tilde{v}^+ and \tilde{v}^- , except the extrapolated plane-wave direct arrival $\tilde{v}_d^+(\mathbf{x}_R, \mathbf{p}, t; x_{3,A})$, which coincides with the last arrival of $\tilde{U}^{-,-}(\mathbf{x}_R, -\mathbf{p}, -t; x_{3,A})$, see Figure 17c. By substituting equation 67 into equation 116 we obtain

$$\tilde{v}_d^+(\mathbf{x}_R, \mathbf{p}, t; x_{3,A}) = \delta(t - \mathbf{p} \cdot \mathbf{x}_{H,R}). \quad (126)$$

Application of the time windows to both sides of equations 120 and 121 gives, in the compact operator notation,

$$\tilde{v}^- = \tilde{\Theta}_b^{\epsilon,v} R \tilde{v}^+, \quad (127)$$

$$\tilde{v}^+ = \tilde{\Theta}_a^v R^* \tilde{v}^- + \tilde{\delta}, \quad (128)$$

where $\tilde{\delta}$ stands for $\tilde{v}_d^+(\mathbf{x}_R, \mathbf{p}, t; x_{3,A}) = \delta(t - \mathbf{p} \cdot \mathbf{x}_{H,R})$. Solving these Marchenko equations for the extrapo-

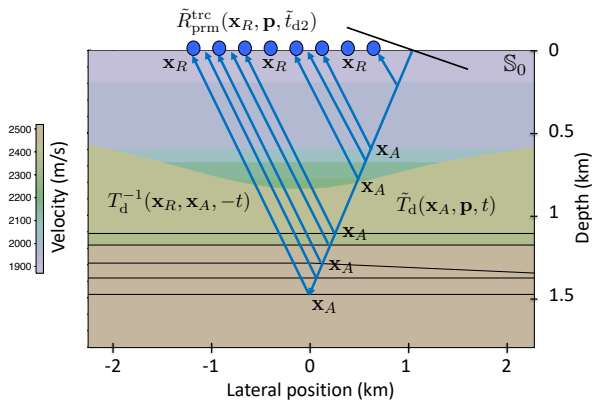


FIG. 18 Visualization of the plane-wave transmission-loss compensated primary response $\tilde{R}_{\text{pr}m}^{\text{tr}c}(\mathbf{x}_R, \mathbf{p}, \tilde{t}_{d2})$, obtained from equations 122, 129 and 130 for all $x_{3,A}$.

lated plane-wave focusing function \tilde{v}^- yields

$$\tilde{v}^-(\mathbf{x}_R, \mathbf{p}, t; x_{3,A}) = \tilde{\Theta}_b^{\epsilon,v} R \sum_{k=0}^K \{ \tilde{\Theta}_a^v R^* \tilde{\Theta}_b^{\epsilon,v} R \}^k \tilde{\delta}. \quad (129)$$

The plane-wave transmission-loss compensated primary reflection response $\tilde{R}_{\text{pr}m}^{\text{tr}c}(\mathbf{x}_R, \mathbf{p}, t)$ can be obtained by evaluating equation 129 for all $x_{3,A}$ and, for each $x_{3,A}$, assigning the time slice $t = \tilde{t}_{d2}(\mathbf{x}_R, \mathbf{p}; x_{3,A})$ to $\tilde{R}_{\text{pr}m}^{\text{tr}c}(\mathbf{x}_R, \mathbf{p}, t)$, according to

$$\tilde{R}_{\text{pr}m}^{\text{tr}c}(\mathbf{x}_R, \mathbf{p}, \tilde{t}_{d2}) = \{ \tilde{v}^-(\mathbf{x}_R, \mathbf{p}, t; x_{3,A}) \}_{t=\tilde{t}_{d2}(\mathbf{x}_R, \mathbf{p}; x_{3,A})}. \quad (130)$$

Since the leftmost window $\tilde{\Theta}_b^{\epsilon,v}$ in equation 129 passes the selected time slice, we may remove this window function from this equation when its output \tilde{v}^- is used in equation 130. Figure 18 visualizes $\tilde{R}_{\text{pr}m}^{\text{tr}c}(\mathbf{x}_R, \mathbf{p}, \tilde{t}_{d2})$ for all $x_{3,A}$.

Next, using similar arguments as in the previous section, we replace the depth variable $x_{3,A}$ again by the two-way travelttime t_2 along the vertical coordinate between $x_{3,0}$ and $x_{3,A}$ (hence, independent of \mathbf{x}_R and \mathbf{p}), and the time window function $\tilde{\Theta}_b^{\epsilon,v}(\mathbf{x}_R, \mathbf{p}, t; x_{3,A})$ by

$$\tilde{\Theta}_b^{\epsilon,v}(\mathbf{x}_R, \mathbf{p}, t; t_2) = \theta(t_2 + \mathbf{p} \cdot \mathbf{x}_{H,R} + \epsilon - t) \quad (131)$$

(Meles et al., 2020). Making these replacements in equations 129 and 130, we obtain

$$\begin{aligned} \tilde{R}_{\text{pr}m}^{\text{tr}c}(\mathbf{x}_R, \mathbf{p}, \tilde{t}_2) &= \{ \tilde{v}^-(\mathbf{x}_R, \mathbf{p}, t; t_2) \}_{t=t_2+\mathbf{p} \cdot \mathbf{x}_{H,R}} \\ &= \left(R \sum_{k=0}^K \{ \tilde{\Theta}_a^v R^* \tilde{\Theta}_b^{\epsilon,v} R \}^k \tilde{\delta} \right)_{t=t_2+\mathbf{p} \cdot \mathbf{x}_{H,R}}. \end{aligned} \quad (132)$$

This equation shows how the plane-wave transmission-loss compensated primary reflection response $\tilde{R}_{\text{pr}m}^{\text{tr}c}(\mathbf{x}_R, \mathbf{p}, \tilde{t}_2)$, with $\tilde{t}_2 = t_2 + \mathbf{p} \cdot \mathbf{x}_{H,R}$, is retrieved from the reflection data at the surface without needing any velocity information. Using this equation as the basis for primary retrieval, the Marchenko method is only needed to retrieve the extrapolated plane-wave focusing function \tilde{v}^- for a limited number of rayparameters at each vertical travelttime. This implies a significant efficiency gain in comparison with primary retrieval based on equation 115, particularly for 3D applications. Meles et al. (2020) discuss applications of plane-wave transmission-loss compensated primary retrieval to 2D numerically modeled data.

DISCUSSION

The last decade has seen vigorous progress in the field of Marchenko-equation-based methods for dealing with internal multiples, be it through redatuming and imaging, or multiple elimination at the surface. The geophysical community has managed to move from understanding the fundamentals and expand on them, through identifying (and resolving) some limitations, to making this suite of methods more user-friendly and more computationally efficient and, finally, to apply them to field data. It is therefore prudent to not only take stock of the collective accomplishments of our community, but also draw a roadmap of attention-worthy research directions. Of those that we were able to identify, we decided to split them up into four main themes: (1) understanding the effects of band limitation, (2) investigating whether the focusing functions or dereverberation operators can be reliably extracted from reflection data for complex subsurface configurations, (3) understanding how the methods fit within a wider data processing workflow and what quality control tools would be needed, and, finally (4) looking beyond the acoustic assumption outlined in this work.

1. We need to close the gap between the theory and real world applications, where the signal bandwidth often tends to be much lower than that of the heterogeneities. This is particularly an issue, since finite bandwidth and temporal truncations do not go well together. For example, Elison et al. (2020) have shown with a numerical example that when the scattering is sufficiently high and band-limited data are used, the focusing functions or dereverberation operators are not recovered with full fidelity. Recently, augmentation to the Marchenko theory suggested the use of additional constraints to further improve the quality of the retrieved solutions. However, the current implementation of this extension has to date only been shown to

work in horizontally layered media. As discussed in Dukalski (2020), the critical minimum-phase reconstruction step can become challenging beyond 1.5D applications, hence requiring further algorithmic developments.

2. For complex subsurface configurations, events originating from deep sections may outpace the ones from up-shallow. This makes retrieving focusing functions or dereverberation operators directly from the reflection data rather difficult. It would be worthwhile to investigate for such situations when one can show that the operators do or do not exist, and to what extent they can be extracted from the reflection data using the data-driven approaches discussed in this work. It might further be worth understanding, should a partially correct operator be found using the schemes we outline here, to what extent it is capable to actually remove the multiples in these complex situations.
3. A large-scale deployment of this methodology will be naturally contingent on one's ability to integrate any of the outlined schemes in the data processing workflow (be it for seismic or medical imaging, or otherwise). For instance, when applied in the subsurface imaging workflow, any application should be preceded by surface-related multiple attenuation (with the exception of deep-water settings), or at least a correct wavelet deconvolution step. Since the Marchenko methods rely on sufficient amplitude fidelity of the input data, strengths and weaknesses of the pre-processing need to be well understood and taken into account. Considering the richness in physics and scattering relations underpinning the Marchenko method, perhaps physics can also be used as a viable quality control step. This will be particularly important in cases where multiples are expressed by a massive collection of interfering events, produced by countless reflectors in the subsurface, and where the interpretation of the generation mechanism of multiples and their order might be very difficult. Perhaps machine learning and/or artificial intelligence applications could be of help. Controlled studies on increasingly complex and realistic numerical data would be very useful in achieving this larger goal.
4. Lastly, next to a surge of publications covering many aspects of the acoustic theory, developments also include visco-acoustic (Slob, 2016) and elastic theory (Wapenaar and Slob, 2014; da Costa Filho et al., 2014; Reinicke et al., 2020). In either of these cases, however, we do not directly measure all data necessary for the algorithms, but perhaps additional constraints could help moving these developments forward.

Moreover, in both the visco-acoustic and elastic settings, the aforementioned band-limitation issues become even more apparent, as so-called 'fast converted multiples', dissipation and short-period scattering manifest themselves in a similar manner, but have completely different origins and hence might need to be handled by different means. Alternatively, if not possible to address one or more of these issues, it will be worth exploring in what parameter regime the acoustic approach performs acceptably (Reinicke et al., 2021) and, when it fails, how one would know in practice that it does (for example due to appearance of some characteristic noise). Further extensions of the theory to increasingly 'exotic' systems might also come with the added benefit of bringing to light certain elements, which would otherwise be easily missed in simpler methods.

Most of the issues mentioned here apply also to other internal multiple elimination methods. We hope that this paper will contribute to an unprejudiced discussion between the proponents of the different methods that will help to move the interesting field of internal multiple elimination forward.

CONCLUSIONS

We have presented recent developments of the Marchenko method for geophysical applications in a systematic way. We distinguished two classes of Marchenko methods. The first class of methods, which we call Marchenko redatuming and imaging, aims at creating virtual sources and receivers in the subsurface, from reflection data at the surface. The responses between these virtual sources and receivers are free of internal multiples related to the overburden and can subsequently be used for multiple-free imaging. Methods in the second class also eliminate internal multiples, but the sources and receivers stay at the surface. We refer to these methods as Marchenko multiple elimination. Whereas Marchenko redatuming and imaging methods need a macro model of the subsurface (to define the direct arrival of the Green's functions), Marchenko multiple elimination methods do not need this kind of information. We have used a systematic presentation and unified notation to reveal the relation between the different Marchenko methods in both classes. Finally, we discussed open problems of Marchenko methods (and other internal multiple elimination methods) and indicated new research directions.

ACKNOWLEDGMENTS

We thank the associate editor and reviewers for their positive and constructive review, which helped to improve the paper. We acknowledge funding from the European Research Council (ERC) under the European Union's Horizon 2020 research and innovation programme (grant agreement No: 742703).

DATA AND MATERIALS AVAILABILITY

No data have been used for this study.

Appendix: Derivation of the representations

We define the Fourier transform of a space- and time-dependent quantity $u(\mathbf{x}, t)$ as

$$u(\mathbf{x}, \omega) = \int_{-\infty}^{\infty} u(\mathbf{x}, t) \exp(i\omega t) dt, \quad (\text{A} - 1)$$

where i is the imaginary unit and ω the angular frequency. Consider an acoustic wave field in the space-frequency domain in an inhomogeneous lossless medium. This wave field can be decomposed into downgoing and upgoing components $p^+(\mathbf{x}, \omega)$ and $p^-(\mathbf{x}, \omega)$, respectively. These fields are mutually coupled due to the inhomogeneities of the medium. We assume that the decomposed fields are normalized with respect to the acoustic power flux (de Hoop, 1992; Garmany, 1983; Kennett et al., 1978; Ursin, 1983). Acoustic sources can also be decomposed into sources for downgoing and upgoing waves, $s^+(\mathbf{x}, \omega)$ and $s^-(\mathbf{x}, \omega)$, respectively.

We define a volume \mathbb{V} , bounded by two infinite horizontal boundaries \mathbb{S}_0 and \mathbb{S}_A , defined by $x_3 = x_{3,0}$ and $x_3 = x_{3,A}$, respectively, with $x_{3,A} > x_{3,0}$. In general the boundaries \mathbb{S}_0 and \mathbb{S}_A do not coincide with physical boundaries. In this volume we consider two independent acoustic states, denoted by subscripts A and B , respectively. The decomposed wave fields and sources in these states are related via the following two reciprocity theorems (Wapenaar, 1996)

$$\begin{aligned} & \int_{\mathbb{V}} \{p_A^+ s_B^- - p_A^- s_B^+ + s_A^+ p_B^- - s_A^- p_B^+\} d\mathbf{x} \\ &= - \int_{\mathbb{S}_0} \{p_A^+ p_B^- - p_A^- p_B^+\} d\mathbf{x} \\ & \quad + \int_{\mathbb{S}_A} \{p_A^+ p_B^- - p_A^- p_B^+\} d\mathbf{x}, \end{aligned}$$

$$(\text{A} - 2)$$

and

$$\begin{aligned} & \int_{\mathbb{V}} \{p_A^+ s_B^{+*} - p_A^- s_B^{-*} + s_A^+ p_B^{+*} - s_A^- p_B^{-*}\} d\mathbf{x} \\ &= - \int_{\mathbb{S}_0} \{p_A^+ p_B^{+*} - p_A^- p_B^{-*}\} d\mathbf{x} \\ & \quad + \int_{\mathbb{S}_A} \{p_A^+ p_B^{+*} - p_A^- p_B^{-*}\} d\mathbf{x}, \end{aligned} \quad (\text{A} - 3)$$

where the asterisk denotes complex conjugation. It is assumed that the medium parameters in states A and B are identical in volume \mathbb{V} ; outside this volume the medium parameters may be different. In equation (A-3) evanescent waves are neglected. We use these reciprocity theorems to derive several equations used in the paper. From here onward we assume that the half-space above \mathbb{S}_0 is homogeneous.

We first derive equations 97 and 98, which formulate relations between the decomposed focusing functions f_1^\pm and f_2^\pm , defined in the truncated medium. This truncated medium is identical to the actual medium above \mathbb{S}_A and reflection free below \mathbb{S}_A . For state A we consider the focusing functions $f_1^\pm(\mathbf{x}, \mathbf{x}_A, t)$, introduced in the section ‘‘Focusing functions’’, with the focusing conditions formulated in equations 2 and 3. For state B we consider the focusing functions $f_2^\pm(\mathbf{x}, \mathbf{x}_R, t)$, introduced in the section ‘‘Transmission-loss compensated primary retrieval’’, with the focusing conditions formulated in equations 94 and 95. These focusing functions, transformed to the space-frequency domain, are listed in Table A1. Substituting the states of Table A1 into equations A-2 and A-3 gives

$$f_1^+(\mathbf{x}_R, \mathbf{x}_A, \omega) = f_2^-(\mathbf{x}_A, \mathbf{x}_R, \omega), \quad (\text{A} - 4)$$

$$f_1^-(\mathbf{x}_R, \mathbf{x}_A, \omega) = -\{f_2^+(\mathbf{x}_A, \mathbf{x}_R, \omega)\}^*. \quad (\text{A} - 5)$$

Transforming these equations back to the space-time domain yields equations 97 and 98.

Next, we derive equations 4 and 5, which formulate relations between the decomposed focusing functions in the truncated medium and the decomposed Green's functions in the actual medium. For state A we consider again the focusing functions $f_1^\pm(\mathbf{x}, \mathbf{x}_A, t)$. For state B we consider the Green's functions $G^{\pm,+}(\mathbf{x}, \mathbf{x}_R, t)$, introduced in the section ‘‘Representations’’, with \mathbf{x}_R at or below \mathbb{S}_0 , hence, $x_{3,R} \geq x_{3,0}$. The source at \mathbf{x}_R is a unit source for downgoing waves, hence, $s_B^+ = \delta(\mathbf{x} - \mathbf{x}_R)$ and $s_B^- = 0$. The Green's functions, transformed to the space-frequency domain, are listed in Table A2. The Heaviside function $\theta(x_{3,0} - x_{3,R})$ accounts for the fact that for \mathbf{x} at \mathbb{S}_0 we have $p_B^+(\mathbf{x}, \omega) = G^{+,+}(\mathbf{x}, \mathbf{x}_R, \omega) = \frac{1}{2}\delta(\mathbf{x}_H - \mathbf{x}_{H,R})$ when \mathbf{x}_R lies at \mathbb{S}_0 and $p_B^+(\mathbf{x}, \omega) =$

$G^{+,+}(\mathbf{x}, \mathbf{x}_R, \omega) = 0$ when \mathbf{x}_R lies below \mathbb{S}_0 . Substituting state A of Table A1 and state B of Table A2 into equations A-2 and A-3, we obtain

$$\begin{aligned} & G^{-,+}(\mathbf{x}_A, \mathbf{x}_R, \omega) \\ & + f_1^-(\mathbf{x}_R, \mathbf{x}_A, \omega) \{ \theta(x_{3,0} - x_{3,R}) + \chi_V(\mathbf{x}_R) \} \\ & = \int_{\mathbb{S}_0} f_1^+(\mathbf{x}, \mathbf{x}_A, \omega) G^{-,+}(\mathbf{x}, \mathbf{x}_R, \omega) d\mathbf{x} \end{aligned} \quad (\text{A-6})$$

and

$$\begin{aligned} & - \{ G^{+,+}(\mathbf{x}_A, \mathbf{x}_R, \omega) \}^* \\ & + f_1^+(\mathbf{x}_R, \mathbf{x}_A, \omega) \{ \theta(x_{3,0} - x_{3,R}) + \chi_V(\mathbf{x}_R) \} \\ & = \int_{\mathbb{S}_0} f_1^-(\mathbf{x}, \mathbf{x}_A, \omega) \{ G^{-,+}(\mathbf{x}, \mathbf{x}_R, \omega) \}^* d\mathbf{x}, \end{aligned} \quad (\text{A-7})$$

where $\chi_V(\mathbf{x})$ the characteristic function for \mathbb{V} , i.e.,

$$\chi_V(\mathbf{x}) = \theta(x_{3,A} - x_3) - \theta(x_{3,0} - x_3). \quad (\text{A-8})$$

Note that

$$\{ \theta(x_{3,0} - x_{3,R}) + \chi_V(\mathbf{x}_R) \} = \theta(x_{3,A} - x_{3,R}). \quad (\text{A-9})$$

TABLE A1. States A and B for the derivation of equations A-4 and A-5.

	State A	State B
\mathbf{x} in \mathbb{V}	$p_A^\pm = f_1^\pm(\mathbf{x}, \mathbf{x}_A, \omega)$ $s_A^\pm = 0$	$p_B^\pm = f_2^\pm(\mathbf{x}, \mathbf{x}_R, \omega)$ $s_B^\pm = 0$
\mathbf{x} at \mathbb{S}_0	$p_A^\pm = f_1^\pm(\mathbf{x}, \mathbf{x}_A, \omega)$	$p_B^+ = 0$ $p_B^- = \delta(\mathbf{x}_H - \mathbf{x}_{H,R})$
\mathbf{x} at \mathbb{S}_A	$p_A^+ = \delta(\mathbf{x}_H - \mathbf{x}_{H,A})$ $p_A^- = 0$	$p_B^\pm = f_2^\pm(\mathbf{x}, \mathbf{x}_R, \omega)$

TABLE A2. State B for the derivation of equations A-6 and A-7.

	State B
\mathbf{x} in \mathbb{V}	$p_B^\pm = G^{\pm,+}(\mathbf{x}, \mathbf{x}_R, \omega)$, $x_{3,R} \geq x_{3,0}$ $s_B^+ = \delta(\mathbf{x} - \mathbf{x}_R)$, $s_B^- = 0$
\mathbf{x} at \mathbb{S}_0	$p_B^+ = \theta(x_{3,0} - x_{3,R}) \delta(\mathbf{x}_H - \mathbf{x}_{H,R})$ $p_B^- = G^{-,+}(\mathbf{x}, \mathbf{x}_R, \omega)$
\mathbf{x} at \mathbb{S}_A	$p_B^\pm = G^{\pm,+}(\mathbf{x}, \mathbf{x}_R, \omega)$

TABLE A3. State B for the derivation of equations A-12 and A-13.

	State B
\mathbf{x} in \mathbb{V}	$p_B^\pm = G^{\pm,-}(\mathbf{x}, \mathbf{x}_R, \omega)$, $x_{3,R} \geq x_{3,0}$ $s_B^+ = 0$, $s_B^- = \delta(\mathbf{x} - \mathbf{x}_R)$
\mathbf{x} at \mathbb{S}_0	$p_B^+ = 0$ $p_B^- = G^{-,-}(\mathbf{x}, \mathbf{x}_R, \omega)$
\mathbf{x} at \mathbb{S}_A	$p_B^\pm = G^{\pm,-}(\mathbf{x}, \mathbf{x}_R, \omega)$

Equations 4 and 5 are derived as follows from equations A-6, A-7 and A-9. Apply the reciprocity relations for the decomposed Green's functions

$$G^{-,+}(\mathbf{x}_A, \mathbf{x}_R, \omega) = G^{-,+}(\mathbf{x}_R, \mathbf{x}_A, \omega), \quad (\text{A-10})$$

$$G^{+,+}(\mathbf{x}_A, \mathbf{x}_R, \omega) = -G^{-,-}(\mathbf{x}_R, \mathbf{x}_A, \omega) \quad (\text{A-11})$$

(Wapenaar, 1996). Next, replace \mathbf{x} by \mathbf{x}_S and take \mathbf{x}_S and \mathbf{x}_R both at \mathbb{S}_0 (hence, $\theta(x_{3,A} - x_{3,R}) = 1$). Define the reflection response at the surface \mathbb{S}_0 as $R(\mathbf{x}_R, \mathbf{x}_S, \omega) = G^{-,+}(\mathbf{x}_R, \mathbf{x}_S, \omega)$. Apply inverse Fourier transforms and limit the time integrals, taking into account that $R(\mathbf{x}_R, \mathbf{x}_S, t)$ is a causal function of time.

Equation 26 is obtained as follows from equation A-6. Replace \mathbf{x}_A by \mathbf{x}_B , \mathbf{x}_R by \mathbf{x}_A and \mathbf{x} by \mathbf{x}_R . Take \mathbf{x}_A and \mathbf{x}_B both at \mathbb{S}_A (hence, the upgoing focusing function is zero, see equation 3). Define the target reflection response at \mathbb{S}_A as $R_{\text{tar}}(\mathbf{x}_B, \mathbf{x}_A, \omega) = G^{-,+}(\mathbf{x}_B, \mathbf{x}_A, \omega)$. Apply inverse Fourier transforms and limit the time integrals, taking into account that $G^{-,+}(\mathbf{x}_R, \mathbf{x}_A, t)$ is a causal function of time.

Finally, we aim to derive equations 33 – 36, for \mathbf{x}_A and \mathbf{x}_B at different depth levels. First, we define another state B for Green's functions $G^{\pm,-}(\mathbf{x}, \mathbf{x}_R, t)$ with a unit source for upgoing waves at \mathbf{x}_R . These Green's functions, transformed to the space-frequency domain, are listed in Table A3. Substituting state A of Table A1 and state B of Table A3 into equations A-2 and A-3, we obtain

$$\begin{aligned} & G^{-,-}(\mathbf{x}_A, \mathbf{x}_R, \omega) \\ & - f_1^+(\mathbf{x}_R, \mathbf{x}_A, \omega) \{ \theta(x_{3,A} - x_{3,R}) - \theta(x_{3,0} - x_{3,R}) \} \\ & = \int_{\mathbb{S}_0} f_1^+(\mathbf{x}, \mathbf{x}_A, \omega) G^{-,-}(\mathbf{x}, \mathbf{x}_R, \omega) d\mathbf{x} \end{aligned} \quad (\text{A} - 12)$$

and

$$\begin{aligned} & \{ G^{+,-}(\mathbf{x}_A, \mathbf{x}_R, \omega) \}^* \\ & + f_1^-(\mathbf{x}_R, \mathbf{x}_A, \omega) \{ \theta(x_{3,A} - x_{3,R}) - \theta(x_{3,0} - x_{3,R}) \} \\ & = - \int_{\mathbb{S}_0} f_1^-(\mathbf{x}, \mathbf{x}_A, \omega) \{ G^{-,-}(\mathbf{x}, \mathbf{x}_R, \omega) \}^* d\mathbf{x}. \end{aligned} \quad (\text{A} - 13)$$

Equations 33 – 36 are obtained from equations A-6, A-7, A-12 and A-13 as follows. Replace \mathbf{x}_A by \mathbf{x}_B , \mathbf{x}_R by \mathbf{x}_A and \mathbf{x} by \mathbf{x}_R . Apply inverse Fourier transforms and limit the time integrals, taking into account that the Green's functions are causal functions of time. Rewrite the resulting expressions in the compact operator notation.

REFERENCES

- Amundsen, L., 2001, Elimination of free-surface related multiples without need of the source wavelet: *Geophysics*, **66**, no. 1, 327–341.
- Bakulin, A. and R. Calvert, 2006, The virtual source method: Theory and case study: *Geophysics*, **71**, no. 4, SI139–SI150.
- Becker, T. S., M. Ravasi, D. J. van Manen, F. Broggini, and J. O. A. Robertsson, 2018, Sparse inversion of the coupled Marchenko equations for simultaneous source wavelet and focusing functions estimation: 80th Annual International Meeting, EAGE, Extended Abstracts, Th–P9–15.
- Behura, J., K. Wapenaar, and R. Snieder, 2014, Autofocus imaging: Image reconstruction based on inverse scattering theory: *Geophysics*, **79**, no. 3, A19–A26.
- Berkhout, A. J. and D. W. van Wulfften Palthe, 1979, Migration in terms of spatial deconvolution: *Geophysical Prospecting*, **27**, no. 1, 261–291.
- Berkhout, A. J. and C. P. A. Wapenaar, 1993, A unified approach to acoustical reflection imaging. Part II: The inverse problem: *Journal of the Acoustical Society of America*, **93**, no. 4, 2017–2023.
- Berkhout, A. J. and D. J. Verschuur, 1997, Estimation of multiple scattering by iterative inversion. Part I. Theoretical considerations: *Geophysics*, **62**, 1586–1595.
- Berkhout, A. J., 1982, *Seismic Migration. Imaging of acoustic energy by wave field extrapolation. A. Theoretical aspects*: Elsevier.
- Berryhill, J. R., 1984, Wave-equation datuming before stack: *Geophysics*, **49**, 2064–2066.
- Brackenhoff, J., J. Thorbecke, and K. Wapenaar, 2019a, Monitoring of induced distributed double-couple sources using Marchenko-based virtual receivers: *Solid Earth*, **10**, 1301–1319.
- 2019b, Virtual sources and receivers in the real Earth: Considerations for practical applications: *Journal of Geophysical Research*, **124**, 11,802–11,821.
- Broggini, F. and R. Snieder, 2012, Connection of scattering principles: a visual and mathematical tour: *European Journal of Physics*, **33**, 593–613.
- Broggini, F., R. Snieder, and K. Wapenaar, 2014, Data-driven wavefield focusing and imaging with multidimensional deconvolution: Numerical examples for reflection data with internal multiples: *Geophysics*, **79**, no. 3, WA107–WA115.
- Campillo, M. and A. Paul, 2003, Long-range correlations in the diffuse seismic coda: *Science*, **299**, 547–549.
- Chapman, C. H., 1994, Reflection/transmission coefficients reciprocities in anisotropic media: *Geophysical Journal International*, **116**, 498–501.
- Cui, T., J. Rickett, I. Vasconcelos, and B. Veitch, 2020, Target-oriented full-waveform inversion using Marchenko redatumed wavefields: *Geophysical Journal International*, **223**, 792–810.
- da Costa Filho, C. A., M. Ravasi, A. Curtis, and G. A. Meles, 2014, Elastodynamic Green's function retrieval through single-sided Marchenko inverse scattering: *Physical Review E*, **90**, 063201.
- de Bruin, C. G. M., C. P. A. Wapenaar, and A. J. Berkhout, 1990, Angle-dependent reflectivity by means of prestack migration: *Geophysics*, **55**, no. 9, 1223–1234.
- de Hoop, M. V., 1992, Directional decomposition of transient acoustic wave fields: Ph.D. thesis, Delft University of Technology.
- Diekman, L. and I. Vasconcelos, 2021, Focusing and Green's function retrieval in three-dimensional inverse scattering revisited: A single-sided Marchenko integral for the full wave field: *Physical Review Research*, **3**, 013206.
- Dukalski, M. and K. de Vos, 2018, Marchenko inversion in a strong scattering regime including surface-related multiples: *Geophysical Journal International*, **212**, 760–776.
- Dukalski, M. and K. de Vos, 2020, A closed formula for true-amplitude overburden-generated interbed demultiple: 82nd Annual International Meeting, EAGE, Extended Abstracts, Fr–P05–18.
- Dukalski, M., E. Mariani, and K. de Vos, 2019, Handling short-period scattering using augmented Marchenko autofocusing: *Geophysical Journal International*, **216**, 2129–2133.
- Dukalski, M., 2020, The role of minimum phase in internal

- multiple removal: 82nd Annual International Meeting, EAGE, Extended Abstracts, WS15–06.
- Elison, P., M. S. Dukalski, K. de Vos, D. J. van Manen, and J. O. A. Robertsson, 2020, Data-driven control over short-period internal multiples in media with a horizontally layered overburden: *Geophysical Journal International*, **221**, 769–787.
- Frasier, C. W., 1970, Discrete time solution of plane P-SV waves in a plane layered medium: *Geophysics*, **35**, 197–219.
- Garmany, J., 1983, Some properties of elastodynamic eigen-solutions in stratified media: *Geophysical Journal of the Royal Astronomical Society*, **75**, 565–569.
- Gouédard, P., L. Stehly, F. Brenguier, M. Campillo, Y. Colin de Verdière, E. Larose, L. Margerin, P. Roux, F. J. Sánchez-Sesma, N. M. Shapiro, and R. L. Weaver, 2008, Cross-correlation of random fields: mathematical approach and applications: *Geophysical Prospecting*, **56**, 375–393.
- Haindl, C. M., F. Brogini, M. Ravasi, and D.-J. van Manen, 2018, Using sparsity to improve the accuracy of Marchenko imaging given imperfect acquisition geometries: 80th Annual International Meeting, EAGE, Extended Abstracts, Th–P9–14.
- Ikelle, L. T., 2006, A construct of internal multiples from surface data only: the concept of virtual seismic events: *Geophysical Journal International*, **164**, 383–393.
- Jakubowicz, H., 1998, Wave equation prediction and removal of interbed multiples: 68th Annual International Meeting, SEG, Expanded Abstracts, 1527–1530.
- Kennett, B. L. N., N. J. Kerry, and J. H. Woodhouse, 1978, Symmetries in the reflection and transmission of elastic waves: *Geophysical Journal of the Royal Astronomical Society*, **52**, 215–230.
- Kiraz, M. S. R., R. Snieder, and K. Wapenaar, 2021, Focusing waves in an unknown 2D medium: *Journal of the Acoustical Society of America*, (in press).
- Lamb, G. L., 1980, *Elements of soliton theory*: John Wiley and Sons, Inc., New York.
- Luiken, N. and T. van Leeuwen, 2020, Seismic wavefield redatuming with regularized multi-dimensional deconvolution: *Inverse Problems*, **36**, 095010.
- Meles, G. A., K. Wapenaar, and A. Curtis, 2016, Reconstructing the primary reflections in seismic data by Marchenko redatuming and convolutional interferometry: *Geophysics*, **81**, no. 2, Q15–Q26.
- Meles, G. A., K. Wapenaar, and J. Thorbecke, 2018, Virtual plane-wave imaging via Marchenko redatuming: *Geophysical Journal International*, **214**, 508–519.
- Meles, G. A., L. Zhang, J. Thorbecke, K. Wapenaar, and E. Slob, 2020, Data-driven retrieval of primary plane-wave responses: *Geophysical Prospecting*, **68**, 1834–1846.
- Mildner, C., M. Dukalski, P. Elison, K. de Vos, F. Brogini, and J. O. A. Robertsson, 2019, True amplitude-versus-offset Green’s function retrieval using augmented Marchenko focusing: 81st Annual International Meeting, EAGE, Extended Abstracts, Tu–R04–08.
- Mulder, W. A., 2005, Rigorous redatuming: *Geophysical Journal International*, **161**, 401–415.
- Peng, H., I. Vasconcelos, Y. Sripanich, and L. Zhang, 2019, On the effects of acquisition sampling on Marchenko-based focusing and primary estimation: 81st Annual International Meeting, EAGE, Extended Abstracts, Th–R08–09.
- Pereira, R., M. Ramzy, P. Griscenco, B. Huard, H. Huang, L. Cypriano, and A. Khalil, 2019, Internal multiple attenuation for OBN data with overburden/target separation: 89th Annual International Meeting, SEG, Expanded Abstracts, 4520–4524.
- Ravasi, M., I. Vasconcelos, A. Kritski, A. Curtis, C. A. da Costa Filho, and G. A. Meles, 2016, Target-oriented Marchenko imaging of a North Sea field: *Geophysical Journal International*, **205**, 99–104.
- Reinicke, C. and M. Dukalski, 2020, Effective media theory consistent multiple elimination with the Marchenko equation based methods: 82nd Annual International Meeting, EAGE, Extended Abstracts, Fr–Dome5–01.
- Reinicke, C., M. Dukalski, and K. Wapenaar, 2020, Comparison of monotonicity challenges encountered by the inverse scattering series and the Marchenko demultiple method for elastic waves: *Geophysics*, **85**, no. 5, Q11–Q26.
- Reinicke, C., M. Dukalski, and K. Wapenaar, 2021, Internal multiple elimination: Can we trust an acoustic approximation?: *Geophysics*, **86** (doi/10.1190/geo2020-0850.1).
- Rietveld, W. E. A., A. J. Berkhout, and C. P. A. Wapenaar, 1992, Optimum seismic illumination of hydrocarbon reservoirs: *Geophysics*, **57**, no. 10, 1331–1345.
- Rose, J. H., 2001, “Single-sided” focusing of the time-dependent Schrödinger equation: *Physical Review A*, **65**, 012707.
- Rose, J. H., 2002, ‘Single-sided’ autofocusing of sound in layered materials: *Inverse Problems*, **18**, 1923–1934.
- Schultz, P. S. and J. F. Claerbout, 1978, Velocity estimation and downward continuation by wavefront synthesis: *Geophysics*, **43**, 691–714.
- Schuster, G. T., J. Yu, J. Sheng, and J. Rickett, 2004, Interferometric/daylight seismic imaging: *Geophysical Journal International*, **157**, 838–852.
- Shoja, S. M. A., G. A. Meles, and K. Wapenaar, 2020, A proposal for Marchenko-based target-oriented full waveform inversion: 82nd Annual International Meeting, EAGE, Extended Abstracts, 1–5.
- Singh, S., R. Snieder, J. van der Neut, J. Thorbecke, E. Slob, and K. Wapenaar, 2017, Accounting for free-surface multiples in Marchenko imaging: *Geophysics*, **82**, no. 1, R19–R30.
- Slob, E., K. Wapenaar, F. Brogini, and R. Snieder, 2014, Seismic reflector imaging using internal multiples with Marchenko-type equations: *Geophysics*, **79**, no. 2, S63–S76.
- Slob, E., 2016, Green’s function retrieval and Marchenko imaging in a dissipative acoustic medium: *Physical Review Letters*, **116**, 164301.
- Staring, M. and K. Wapenaar, 2020, Three-dimensional Marchenko internal multiple attenuation on narrow azimuth streamer data of the Santos Basin, Brazil: *Geophysical Prospecting*, **68**, 1864–1877.
- Staring, M., R. Pereira, H. Douma, J. van der Neut, and K. Wapenaar, 2018, Source-receiver Marchenko redatuming on field data using an adaptive double-focusing method: *Geophysics*, **83**, no. 6, S579–S590.
- Staring, M., M. Dukalski, M. Belonosov, R. H. Baardman, J. Yoo, R. F. Hegge, R. van Borselen, and K. Wapenaar, 2021, Robust estimation of primaries by sparse inversion and Marchenko equation-based workflow for multiple suppression in the case of a shallow water layer and a complex overburden: A 2D case study in the Ara-

- bian Gulf: *Geophysics*, **86**, no. 2, Q15–Q25.
- Taner, M. T., 1976, Simplan: simulated plane-wave exploration: 46th Annual International Meeting, SEG, Expanded Abstracts, 186–187.
- ten Kroode, F., 2002, Prediction of internal multiples: *Wave Motion*, **35**, 315–338.
- Thorbecke, J., L. Zhang, K. Wapenaar, and E. Slob, 2021, Implementation of the Marchenko multiple elimination algorithm: *Geophysics*, **86**, no. 2, F9–F23.
- Ursin, B., 1983, Review of elastic and electromagnetic wave propagation in horizontally layered media: *Geophysics*, **48**, 1063–1081.
- van Borselen, R., 2002, Fast-track, data-driven interbed multiple removal — A North Sea data example: 64th Annual International Meeting, EAGE, Extended Abstracts, F–40.
- van der Neut, J. and K. Wapenaar, 2016, Adaptive overburden elimination with the multidimensional Marchenko equation: *Geophysics*, **81**, no. 5, T265–T284.
- van der Neut, J., J. Thorbecke, K. Mehta, E. Slob, and K. Wapenaar, 2011, Controlled-source interferometric redatuming by crosscorrelation and multidimensional deconvolution in elastic media: *Geophysics*, **76**, no. 4, SA63–SA76.
- van der Neut, J., J. Thorbecke, K. Wapenaar, and E. Slob, 2015a, Inversion of the multidimensional Marchenko equation: 77th Annual International Meeting, EAGE, Extended Abstracts, We–N106–04.
- 2015b, On Green’s function retrieval by iterative substitution of the coupled Marchenko equations: *Geophysical Journal International*, **203**, 792–813.
- 2015c, An illustration of adaptive Marchenko imaging: *The Leading Edge*, **34**, 818–822.
- van der Neut, J., J. L. Johnson, K. van Wijk, S. Singh, E. Slob, and K. Wapenaar, 2017, A Marchenko equation for acoustic inverse source problems: *Journal of the Acoustical Society of America*, **141**, no. 6, 4332–4346.
- van Groenestijn, G. J. A. and D. J. Verschuur, 2010, Estimation of primaries by sparse inversion from passive seismic data: *Geophysics*, **75**, no. 4, SA61–SA69.
- van IJsseldijk, J. and K. Wapenaar, 2021, Adaptation of the iterative Marchenko scheme for imperfectly sampled data: *Geophysical Journal International*, **224**, 326–336.
- Vasconcelos, I. and Y. Sripinich, 2019, Scattering-based Marchenko for subsurface focusing and redatuming in highly complex media: 81st Annual International Meeting, EAGE, Extended Abstracts, Tu–R04–06.
- Vasconcelos, I., K. Wapenaar, J. van der Neut, C. Thomson, and M. Ravasi, 2015, Using inverse transmission matrices for Marchenko redatuming in highly complex media: 85th Annual International Meeting, SEG, Expanded Abstracts, 5081–5086.
- Verschuur, D. J. and A. J. Berkhout, 2005, Removal of internal multiples with the common-focus-point (CFP) approach: Part 2 — Application strategies and data examples: *Geophysics*, **70**, no. 3, V61–V72.
- Verschuur, D. J., A. J. Berkhout, and C. P. A. Wapenaar, 1992, Adaptive surface-related multiple elimination: *Geophysics*, **57**, no. 9, 1166–1177.
- Wapenaar, K. and E. Slob, 2014, On the Marchenko equation for multicomponent single-sided reflection data: *Geophysical Journal International*, **199**, 1367–1371.
- Wapenaar, C. P. A., N. A. Kinneging, and A. J. Berkhout, 1987, Principle of prestack migration based on the full elastic two-way wave equation: *Geophysics*, **52**, no. 2, 151–173.
- Wapenaar, K., J. Thorbecke, J. van der Neut, F. Broggini, E. Slob, and R. Snieder, 2014, Green’s function retrieval from reflection data, in absence of a receiver at the virtual source position: *Journal of the Acoustical Society of America*, **135**, no. 5, 2847–2861.
- Wapenaar, K., J. Thorbecke, J. van der Neut, E. Slob, and R. Snieder, 2017, Review paper: Virtual sources and their responses, Part II: data-driven single-sided focusing: *Geophysical Prospecting*, **65**, 1430–1451.
- Wapenaar, K., J. Brackenhoff, and J. Thorbecke, 2019, Green’s theorem in seismic imaging across the scales: *Solid Earth*, **10**, 517–536.
- Wapenaar, K., R. Snieder, S. de Ridder, and E. Slob, 2021, Green’s function representations for Marchenko imaging without up/down decomposition: *Geophysical Journal International*, (submitted).
- Wapenaar, C. P. A., 1996, One-way representations of seismic data: *Geophysical Journal International*, **127**, 178–188.
- Wapenaar, K., 2003, Synthesis of an inhomogeneous medium from its acoustic transmission response: *Geophysics*, **68**, 1756–1759.
- Ware, J. A. and K. Aki, 1969, Continuous and discrete inverse-scattering problems in a stratified elastic medium. I. Plane waves at normal incidence: *Journal of the Acoustical Society of America*, **45**, no. 4, 911–921.
- Weglein, A. B., F. A. Gasparotto, P. M. Carvalho, and R. H. Stolt, 1997, An inverse-scattering series method for attenuating multiples in seismic reflection data: *Geophysics*, **62**, no. 6, 1975–1989.
- Weglein, A. B., F. V. Araújo, P. M. Carvalho, R. H. Stolt, K. H. Matson, R. T. Coates, D. Corrigan, D. J. Foster, S. A. Shaw, and H. Zhang, 2003, Inverse scattering series and seismic exploration: *Inverse Problems*, **19**, R27–R83.
- Zhang, L. and E. Slob, 2020a, A fast algorithm for multiple elimination and transmission compensation in primary reflections: *Geophysical Journal International*, **221**, 371–377.
- 2020b, A field data example of Marchenko multiple elimination: *Geophysics*, **85**, no. 2, S65–S70.
- Zhang, L., J. Thorbecke, K. Wapenaar, and E. Slob, 2019a, Data-driven internal multiple elimination and its consequences for imaging: A comparison of strategies: *Geophysics*, **84**, no. 5, S365–S372.
- 2019b, Transmission compensated primary reflection retrieval in the data domain and consequences for imaging: *Geophysics*, **84**, no. 4, Q27–Q36.